

CHAPTER 4

EXPERIMENTATION ON DOUBLE PIPE HEAT EXCHANGER

In this chapter, the experimental studies on various mono and hybrid nanofluid flowing under the turbulent condition in a double tube heat exchanger with various modified V-cuts twisted tape and modified tapered wire coil inserts are performed to study the hydrothermal characteristics. It presents the establishment of an experimental setup and geometry of various enhancers for the investigation on the double pipe heat exchanger and the test procedure for different operating parameters. In addition, it has data analyses based on the energy and exergy methodologies and uncertainty analyses. Last but not least, a detailed explanation of the results obtained in terms of different performance parameters has also been presented.

4.1 Experimental setup and procedure

The schematic outline and photograph of the test facility, mainly consisting of the test section (double tube heat exchanger) and flow loops, are shown in Fig. 4.1 (a) and (b). The inlet temperature of hot fluid is adjusted by an electric heater attached to the heating tank with a temperature controller. The chiller, attached with a cold tank, is used for cooling the warm fluid. Two centrifugal pumps were used to drive both fluids in the heat exchanger. Working fluid (mono/hybrid nanofluid) is fed through the inner tube and DI water is passed through annulus in the opposite direction. The inner tube has internal and external diameters of 18 and 26 mm, respectively, whereas the annulus has an internal diameter of 47 mm. The outer tube was wrapped with an asbestos rope to decrease the heat losses to the surrounding. The temperatures of both fluids were determined by using PT-100 thermometers with an accuracy of ± 0.33 %. The range of PT-100 thermometers is from 0 to 250°C. Calibration of

all the thermometers was done with a portable calibrator before fixing them. Two rotameters (one is float type and the other is turbine type) with an accuracy of $\pm 0.67\%$ were installed with control valves in each circular loop to determine the flow rates of the fluids. The range of float type rotameter is from 3.33 lpm to 33.33 lpm, while the range of turbine type rotameter is 0 to 60 lpm, respectively. The control valves were implemented to regulate the flow rate of both fluids. A glass U-tube is fixed against a vertical scale board of length 30 cm. Pressure drop was evaluated by using U-tube manometers inserted between the inlet and outlet of the tubes because of their simplicity and reliability in the operating conditions of the present study. The manometric liquid used in U-tube is mercury. In each test run, all the temperatures and pressure drops were recorded at a period of 15-20 min to ensure the steady-state. The specifications of the double pipe heat exchanger and the range and accuracy of instruments are summarized in Table 4.1.

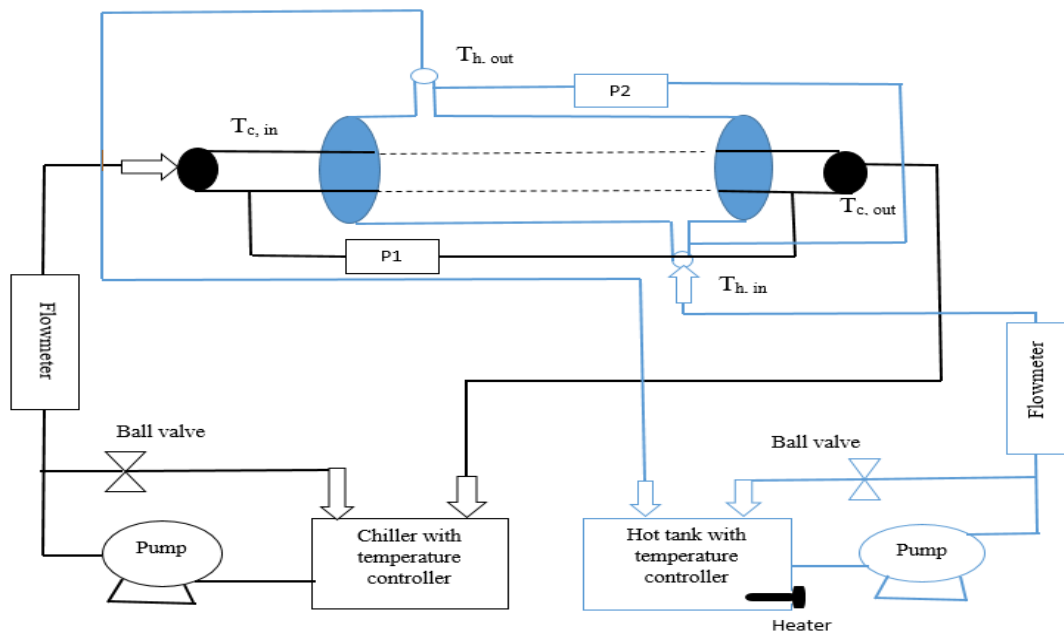


Figure 4.1 (a) Schematic diagram of the experimental setup



Figure 4.1 (b) Actual picture of the test setup

Table 4.1. Details of the experimental setup

Parameter	Value
Inner tube internal diameter	18 mm
Inner tube external diameter	26 mm
Length of the tube	570 mm
Outer tube internal diameter	47 mm
Chiller	3 KW
Heater	2 KW
Pump	80 W, Head up to 7 m
Rotameters	Turbine type (0-60 lpm) Float type (3.33-33.33 lpm) Accuracy= $\pm 0.67\%$
Thermocouples	PT-100, Range = 0-250°C, Accuracy= $\pm 0.33\%$
U-tube Manometer	Mercury height (0-30 cm) Accuracy= $\pm 2.38\%$

4.1.1 Geometry of V-cuts twisted tape

The photograph of V-cut twisted tapes with different twist ratios (TR), i.e., $H/D = 5, 10$ and 15 ; where, H is the pitch of the tapes as shown in Fig.4.2. The twisted tape has been prepared from the 1mm thickness and 15 mm width (D) of aluminum strip. V-cuts were made in the plain twisted tapes on the upper and lower consecutively in the bordering region with different depth and width. Different depth ratios (DR), i.e., P_e/D ($1/2$ and $1/3$) and width ratios (WR), i.e., w/D ($1/2$ and $1/3$) are used. The configurations used in this study are (i) $DR=1/2$ and $WR=1/2$, (ii) $DR=1/3$ and $WR=1/2$ and (iii) $DR=1/3$ and $WR=1/2$. Details of V-cuts twisted tapes are summarized in Table 4.2.



Figure 4.2. V-cuts twisted tape with different TR, DR and WR

Table 4.2. Details of twisted tape and its geometry

Parameter	Value
Tape width	15 mm
Tape thickness	1 mm
Twist ratio (TR= H/D)	5, 10 and 15
Depth of the V-cuts (P_e)	5 and 7.5 mm

Width of the V-cuts (w)	5 and 7.5 mm
Depth ratio ($DR= P_e/D$)	1/2 and 1/3
Width ratio ($WR= w/D$)	1/2 and 1/3

4.1.2 Geometry of tapered wire coil inserts

Three novel tapered wire coil inserts, i.e., convergent type (C-type), divergent type (D-type) and convergent-divergent type (C-D type) are proposed as turbulator in this study. The pictorial view of the plane and tapered wire coil with different configurations, namely convergence type wire coil (C-type), divergence type wire coil (D-type) and convergence-divergence type wire coil (C-D type) as shown in Fig 4.3. A plane wire coil of a constant diameter of 13 mm and a constant pitch of 10 mm is made of aluminium. The tapered wire coil is made with 13 mm diameter (D) from one end and a 6.5 mm diameter ($d=D/2$) from another end with a constant pitch of 10 mm. All the dimensions of the wire coil were measured by using Vernier caliper with the least count of 0.02 mm. The geometry of the tapered wire coil is summarized in Table 4.3.

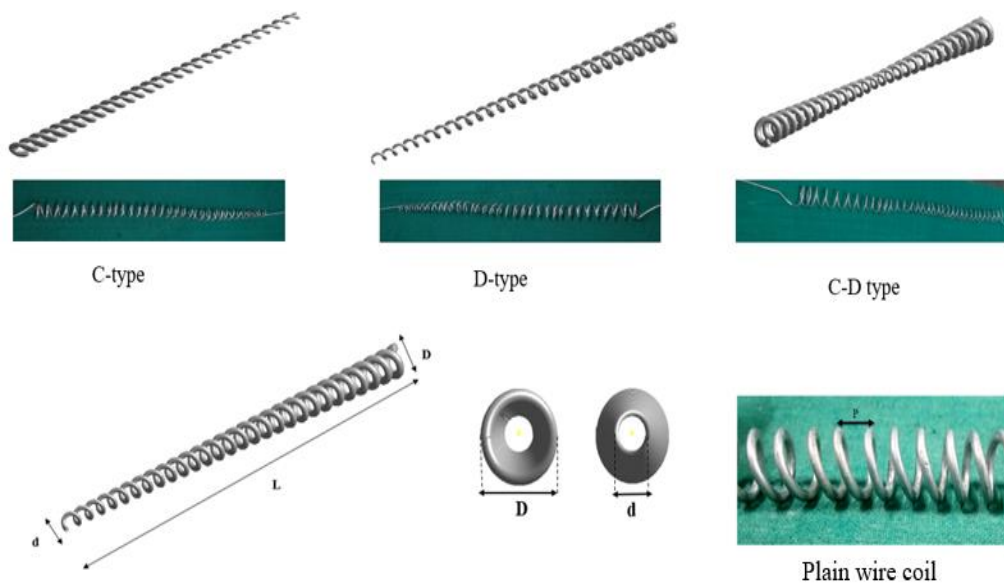


Figure 4.3. Tapered wire coil with different configurations and dimensions

Table 4.3. Details of the tapered wire coil and its geometry

Parameter	Value
Wire thickness	2 mm
Pitch of the tapered wire coil, P	10mm
Larger end diameter of tapered wire coil, D	13 mm
Smaller end diameter of tapered wire coil, d	6.5 mm

4.2 Data reduction

4.2.1 Mono/Hybrid nanofluid as a coolant

Various mono/hybrid nanofluid (Al_2O_3 , PCM, CNT, Al_2O_3 +PCM and Al_2O_3 +CNT) were used as a coolant in the range of volume concentration of 0.01-0.1%. The temperature of mono/hybrid nanofluid in the cold tank was maintained at 30°C by adjusting with the chiller unit and flow rate ranging from 5-25 lpm. The volumetric flow rate of the hybrid nanofluid was controlled by adjusting the ball valve. The hot fluid was supplied through annulus at a constant temperature of 60°C with a constant flow rate of 15 lpm. In the experiment, an enhancer was equipped with inner tube of the double pipe heat exchanger where the coolant was fed through the circulating pump. The Reynolds number of the coolants varies from 8000 to 40000. The operating conditions are summarized in Table 4.4.

Table 4.4. Details of operating conditions when mono and hybrid nanofluids as a coolant

Parameter	Value
Nanofluid flow rate	5-25 lpm
Hot fluid flow rate	15 lpm
Nanofluid inlet temperature	30°C
Hot fluid inlet temperature	60°C
Nanofluid Reynolds number	8000 to 40000

Mono/hybrid nanofluid heat transfer rate in the inner tube is calculated by,

$$q_{nf} = \dot{V}_{nf} \rho_{nf} c_{p,nf} (T_{nf,out} - T_{nf,in}) \quad (4.1)$$

In the case of phase change material (PCM), the hybrid nanofluid heat transfer rate is calculated by,

$$q_{nf} = \dot{V}_{nf} \rho_{nf} c_{p,nf} (T_{nf,out} - T_{nf,in}) + \phi_{PCM} \dot{V}_{nf} \rho_{PCM,solid} L_{PCM} \quad (4.2)$$

Where L_{PCM} is the latent heat of the PCM and \dot{V}_{nf} is volume flow rate.

Hot fluid (DI water) heat transfer rate in the outer tube is calculated by,

$$q_h = \dot{V}_h \rho_h c_{p,h} (T_{h,in} - T_{h,out}) \quad (4.3)$$

Experimentally, there is some difference in the values of q_{nf} and q_h . To ensure the accuracy of the results, the average heat transfer rate is taken, which is determined by,

$$q_{avg} = (q_{nf} + q_h) / 2 \quad (4.4)$$

Equation (4.5) is used to estimate the overall heat transfer coefficient for the inner tube side,

$$U_i = \frac{q_{avg}}{A_i \times \Delta T_{LMTD}}, \quad \Delta T_{LMTD} = \frac{(T_{h,in} - T_{nf,out}) - (T_{h,out} - T_{nf,in})}{\ln \left(\frac{T_{h,in} - T_{nf,out}}{T_{h,out} - T_{nf,in}} \right)} \quad (4.5)$$

Heat transfer coefficient (hybrid nanofluid) without considering fouling can be estimated by,

$$\frac{1}{U_i A_i} = \frac{1}{h_i A_i} + \frac{\ln \left(\frac{d_o}{d_i} \right)}{2\pi k L} + \frac{1}{h_o A_o} \quad (4.6)$$

Nusselt number of annulus side is calculated by using correlation (**Dirker and Mayer, 2002**),

$$Nu_o = 0.007435 Re^{0.91} Pr^{1/3} \left(\frac{\mu}{\mu_w} \right)^{0.14} \quad (4.7)$$

Range: $4000 < Re < 30000$, $1.72 < d_{ot,i}/d_{it,o} < 3.2$

From equations (4.7) and (4.8), the heat transfer coefficient of the outer tube can be calculated,

$$h_o = \frac{Nu_o \times k_o}{d_{eqv}} \quad (4.8)$$

Where d_{eqv} is the equivalent diameter of the outer tube and given by;

$$d_{eqv} = \left(d_{ot,i}^2 - d_{it,o}^2 \right) / d_{it,o} \quad (4.9)$$

The value of h_o from the equation (4.8) is substituted in the equation (4.6), to estimate the inner tube side heat transfer coefficient (h_i or h_{nf}). The Nusselt number of mono/hybrids nanofluid can be measured by the following equation:

$$Nu_{nf} = h_{nf} d_{it,i} / k_{nf} \quad (4.10)$$

The expression for the friction factor is given below;

$$f = \frac{\pi^2}{8} \Delta p \left(\frac{\rho_{nf} d_{it,i}^5}{\dot{m}_{nf}^2 L} \right) \quad (4.11)$$

There are two types of irreversibilities present in the heat exchanger, caused due to heat transfer and fluid friction (frictional pressure drop). By taking a heat exchanger as an adiabatic system, entropy generation has been obtained as an entropy change of both fluids. Then, the second Tds equation has been used for both fluids individually, which is applicable for both reversible and irreversible processes as all these quantities represent state variables. After taking the integration of Tds equation for both fluids and replacing in entropy generation equation, heat transfer and frictional pressure drop parts have been separated.

Hence, the heat transfer related entropy generation has been calculated by,

$$S_{gen_{ht}} = \dot{m}_{nf} c_{pnf} \ln \left(\frac{T_{nf,out}}{T_{nf,in}} \right) + \dot{m}_h c_{ph} \ln \left(\frac{T_{h,out}}{T_{h,in}} \right) \quad (4.12)$$

The pressure drop related entropy generation has been calculated by,

$$S_{gen_f} = \frac{\dot{m}_{nf} \times \Delta p_{nf}}{\rho_{nf} \times T_{avg,nf}} + \frac{\dot{m}_h \times \Delta p_h}{\rho_h \times T_{avg,h}} \quad (4.12a)$$

The total entropy generation for heat transfer can be expressed as follow;

$$S_{gen_{tot}} = m_{nf} c_{p_{nf}} \ln \left(\frac{T_{nf,out}}{T_{nf,in}} \right) + \frac{m_{nf} \times \Delta p_c}{\rho_{nf} \times T_{avg,c}} + m_h c_{p_h} \ln \left(\frac{T_{h,out}}{T_{h,in}} \right) + \frac{m_h \times \Delta p_h}{\rho_h \times T_{avg,h}} \quad (4.12b)$$

4.2.2 Hybrid nanofluid as hot fluid

The experimental studies on Al₂O₃+TiO₂ and Al₂O₃+MgO hybrid nanofluid as a hot fluid flowing under the turbulent condition in a double tube heat exchanger with various enhancers are performed to study the hydrothermal characteristics. Hot fluids (hybrid nanofluid) flows through the inner tube and cold fluid (DI water) flows through annulus in the counter flow direction. In the experiment, the temperature of the cold stream has been kept at 30°C and the flow rate has been maintained at 25 lpm. The hot stream was made to flow through the inner tube where an enhancer was equipped at a constant temperature of 50°C, 60°C and 70°C with different Reynolds number from 8000-40000. The operating condition is summarized in Table 4.5.

Table 4.5. Details of operating conditions when mono and hybrid nanofluids as a hot fluid

Parameter	Value
Nanofluid Reynolds number	8000 to 40000
Nanofluid inlet temperature	50°C, 60°C and 70°C
Cold fluid inlet temperature	30°C
Cold fluid flow rate	25 lpm

Similar analyses have been conducted where hybrid nanofluid has been used as a hot fluid and DI water as a cold fluid. The correlation for the DI water will remain the same as in the

previous case (as a coolant). Further procedure and formulae are the same for calculating other variables, as in the case of mono and hybrid nanofluids as a coolant.

4.3 Uncertainty analysis and validation

4.3.1 Uncertainty analysis

The error analysis of obtained parameters can be estimated by using equations (**Kline and McClintock, 1953**).

$$\frac{\delta X}{X} = \sqrt{\left(\frac{\delta x_1}{x_1}\right)^2 + \left(\frac{\delta x_2}{x_2}\right)^2 + \dots + \left(\frac{\delta x_n}{x_n}\right)^2} \quad (4.13)$$

Appendix A presents the standard procedure for the evaluation of the uncertainty values of the obtained parameters. Based on the accuracies of measured variables and properties, the uncertainty values of estimated parameters such as Re, q, U, h, Nu, f, and S_{gen} are presented in Table 4.6.

Table 4.6. Uncertainty of parameters

Parameter	Uncertainty (%)
Temperature, T	± 0.33
Density, ρ	± 1
Viscosity, μ	± 1
Thermal conductivity, k	± 1
Reynolds number, Re	± 1.22
Heat transfer rate, q	± 1.27
Overall heat transfer coefficient, U	± 1.31
Heat transfer coefficient, h	± 2.13
Nusselt number, Nu	± 2.35
Friction factor, f	± 6.45
Entropy generation, S_{gen}	± 6.10

4.3.2 Validation for DI water

In the beginning, the experiment was conducted with a plain tube using DI water and the results obtained were compared with standard correlation proposed by different authors (**Incopera et al., 2006; Nanan et al., 2014**) for Nusselt number and friction factor as shown in Figs. 4.4 and 4.5.

Sieder and Tate correlation;

$$Nu = 0.027Re^{0.8}Pr^{0.33}\left(\frac{\mu}{\mu_s}\right)^{0.14} \quad (4.14)$$

Nanan et al. correlation;

$$Nu = 0.0068Re^{0.92}Pr^{0.4} \quad (4.15)$$

$$f = 1.01Re^{-0.37} \quad (4.16)$$

The results show that the experimental data are in reasonable agreement with the Sieder-Tate and Nanan et al. correlations for Nusselt number with an average deviation of $\pm 12.9\%$ and $\pm 9.5\%$, respectively. The friction factor is agreed well with the Nanan et al. correlation with an average deviation of $\pm 6.4\%$. Moreover, to gain confidence in the experimental data, the experimental apparatus is also validated by performing the experiments with DI water flowing in the tube inserted with the plain twisted tape of TR =10. Parameters such as temperatures and pressure drop were measured by varying the flow rate from 5 to 25 lpm after reaching steady-state for determining the heat transfer coefficient and friction factor. The experimental Nu and f were calculated using the equations (4.10) and (4.11). The experimental outcomes were compared with the correlations (4.17) and (4.18) (**Manglik and Bergles, 1993**), as predicted in Figs. 4.6 and 4.7. It can be concluded that the

experimental data were in good agreement with the correlations and exhibited a maximum deviation of 5.68% for Nusselt number and 5.55% for friction factor.

$$Nu = \left(1 + \frac{0.769}{TR}\right) \left[0.023 Re^{0.8} Pr^{0.4} \times \left(\left(\frac{\pi}{\pi - \left(\frac{4\delta}{d_i}\right)} \right)^{0.8} \left(\frac{\pi + 2 - \left(\frac{2\delta}{d_i}\right)^{0.2}}{\pi - \left(\frac{4\delta}{d_i}\right)} \right) \right) \right] \quad (4.17)$$

$$f = \left(1 + 2.06 \left(1 + \left(\frac{2TR}{\pi}\right)^2\right)^{-0.74}\right) \left[0.079 Re^{-0.25} \times \left(\frac{\pi}{\pi - \left(\frac{4\delta}{d_i}\right)} \right)^{1.75} \left(\frac{\pi + 2 - \left(\frac{2\delta}{d_i}\right)^{1.25}}{\pi - \left(\frac{4\delta}{d_i}\right)} \right) \right] \quad (4.18)$$

Where δ is the tape thickness.

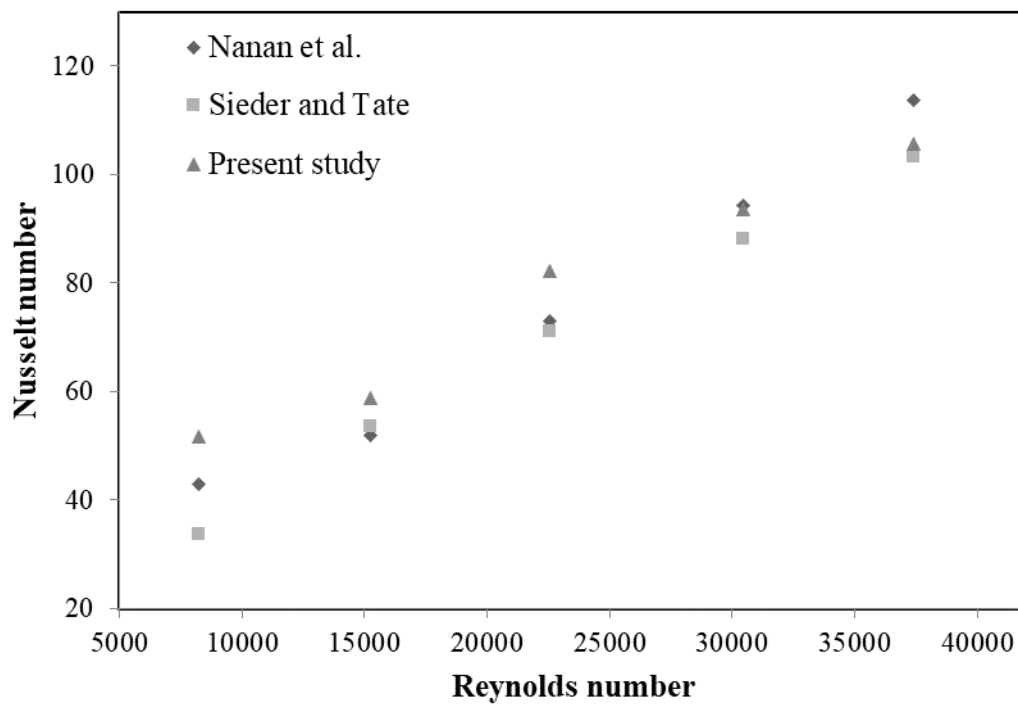


Figure 4.4. Validation of Nusselt number using water with plain tube

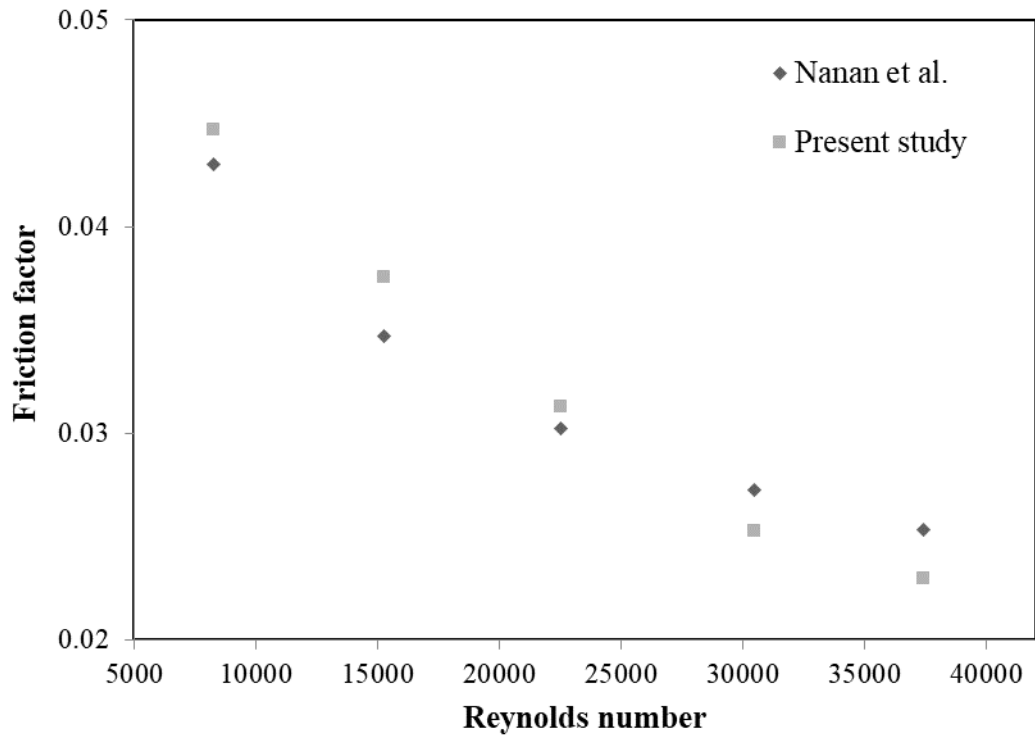


Figure 4.5. Validation of friction factor using water with plain tube

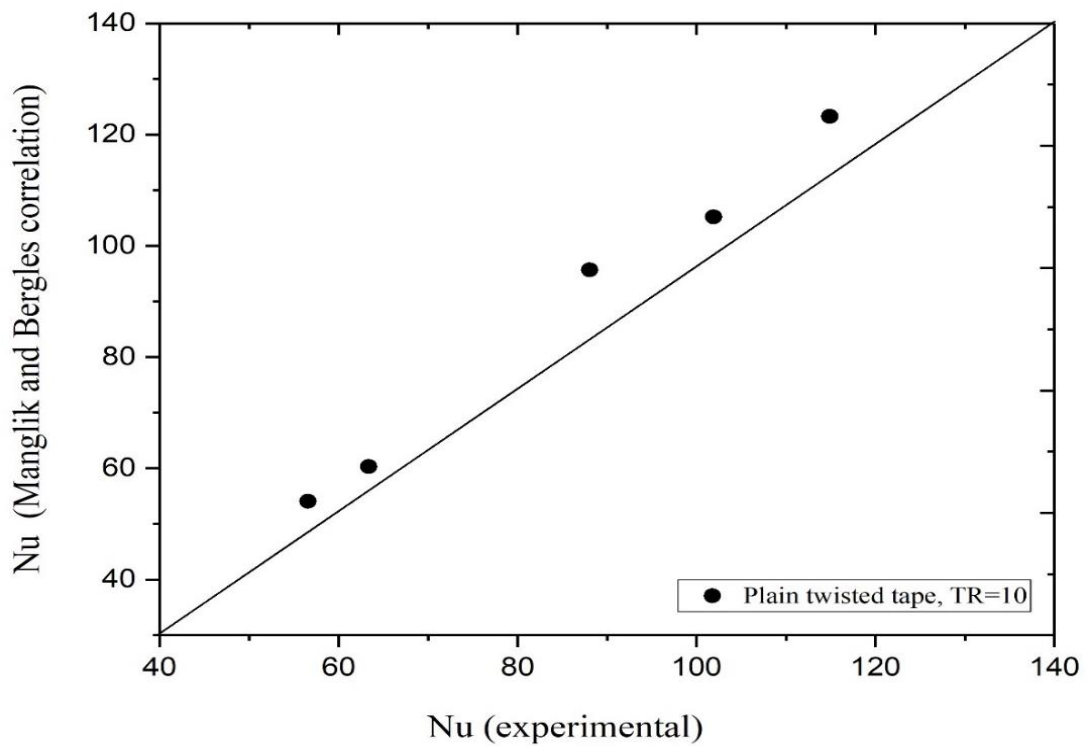


Figure 4.6. Validation of Nussult number using water with plain twisted tape

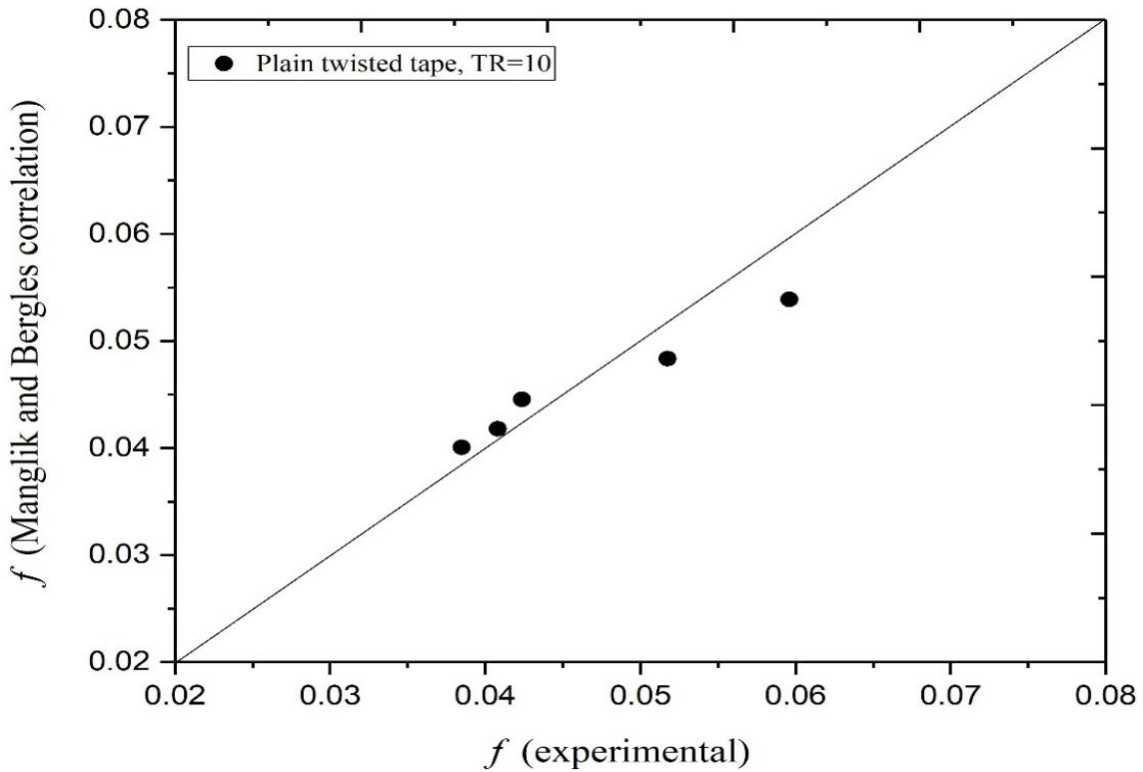


Figure 4.7. Validation of friction factor using water with plain twisted tape

4.4 Results and discussion

4.4.1 Experiment with V-cuts twisted tape inserts

4.4.1.1 Comparison of various mono/hybrid nanofluids

Figs. 4.8 and 4.9 show the influence of various mono and hybrid nanofluid on the heat transfer coefficient (h_i) and pressure drop (Δp) with mean twist ratio (TR=10) and constant depth and width ratios (DR=1/2, WR=1/2) at volume concentration of 0.01%. The results indicate that h_i and Δp considerably increase with an increase in the nanofluid flow rate. In addition, h_i and Δp are greater than that of the DI water. The possible reasons for enhancement due to translational Brownian motion, increase in thermal conductivity, reduction of boundary layer thickness and increase in effective heat transfer surface area due to suspended solid particles. With the addition of nanoparticles in the base fluid, it increases the fluid viscosity, which is the key factor for the enhancement of the pressure drop. The

maximum values of h_i and Δp are observed as 5709.6 W/m²K and 2134.6, respectively, for Al₂O₃+CNT hybrid nanofluid at a higher flow rate (25 lpm). Also, an increment of about 42.77% in heat transfer coefficient and 29.21% in pressure drop for Al₂O₃+CNT hybrid nanofluid as compared to DI water. Also, the results reveal that PCM based mono/hybrid nanofluid, PCM shows a higher heat transfer coefficient at a low flow rate. The coolant has a longer time to absorb heat from the hot fluids at a low flow rate and increases the phase change processes completely, which increases the heat transfer of the coolant and energy storage in PCM particles as the latent heat. At a higher flow rate, PCM show higher pressure drop due to the increased dynamic viscosity by the addition of phase change particles.

Figs. 4.10 and 4.11 show the effect of using various mono and hybrid nanofluid at a volume concentration of 0.01% on the Nusselt number and friction factor with V-cut twisted tape of the same twist ratio and the constant depth and width ratios (DR=1/2, WR=1/2). The results indicate that while increasing Reynolds number, Nu increases due to the similar trend of heat transfer coefficient and f decreases due to an increase of fluid viscosity. The Nusselt number and friction factor of all working fluids are higher than those of the base fluid (DI water) because of the occurrence of solid nanoparticles in the base fluid. As compared to the water, the average enhancement of Nusselt number of 0.01 vol% mono and hybrid nanofluid is 42.22% for Al₂O₃+CNT, 37.36% for CNT, 20.61% for Al₂O₃+PCM, 17.92 % for PCM and 12.10 % for Al₂O₃, while the average enhancement of friction factor is 39.96% for Al₂O₃+CNT, 32.70 % for CNT, 23.27 % for PCM, 20.23 % for Al₂O₃+PCM and 11.98% for Al₂O₃ respectively, for the same twist ratio and same depth and width ratios (DR=1/2, WR=1/2).

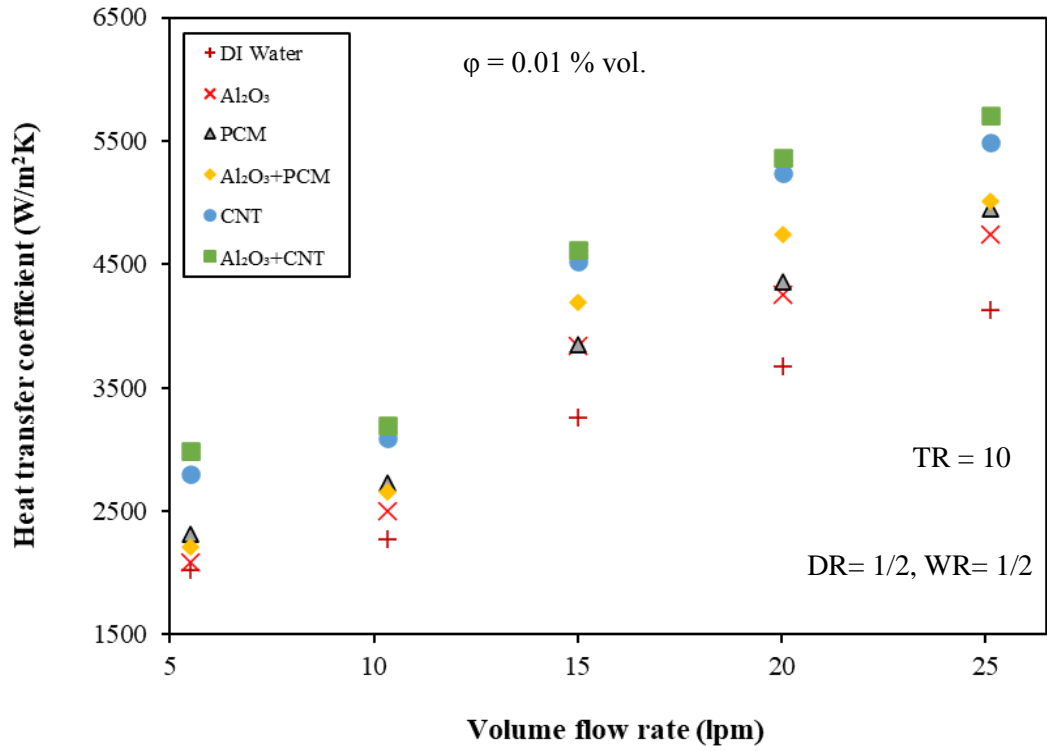


Figure 4.8 Variation of heat transfer coefficient with the nanofluid flow rate

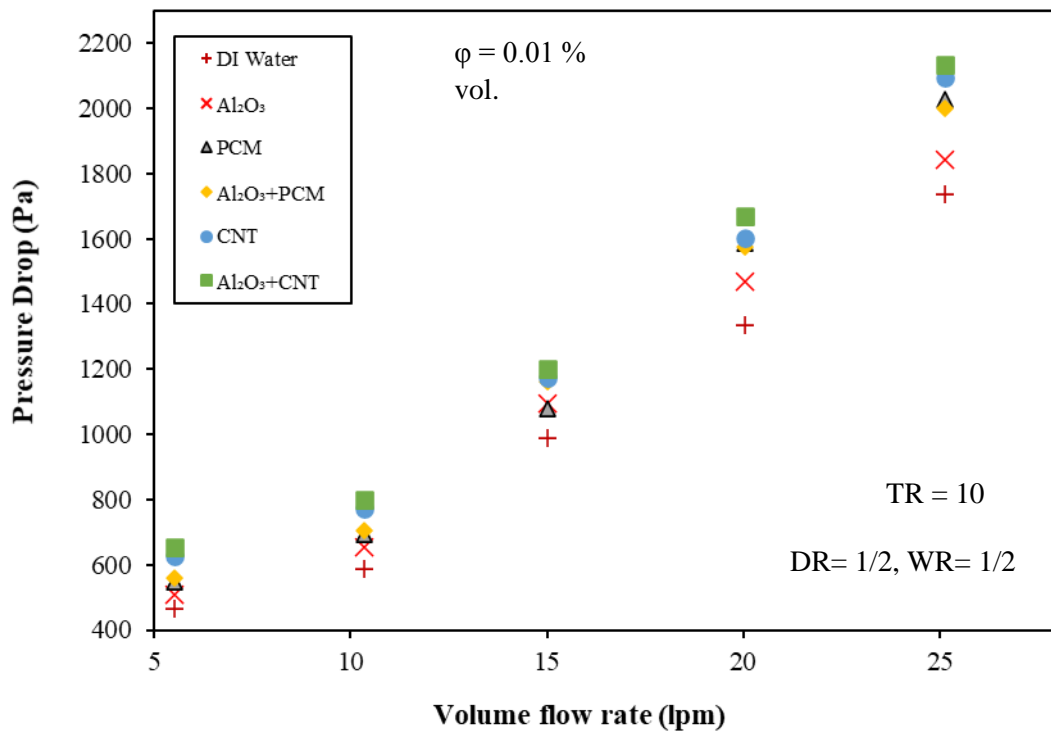


Figure 4.9. Variation of pressure drop with nanofluid flow rate for different nanofluids

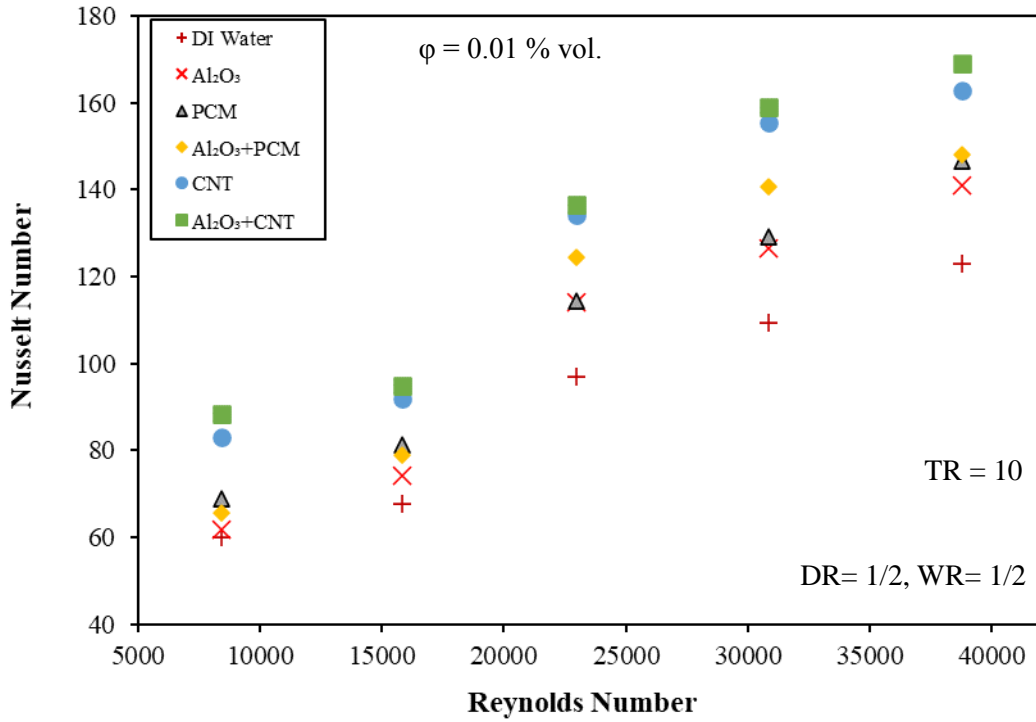


Figure 4.10. Variation of Nusselt number with nanofluid flow rate for different nanofluids

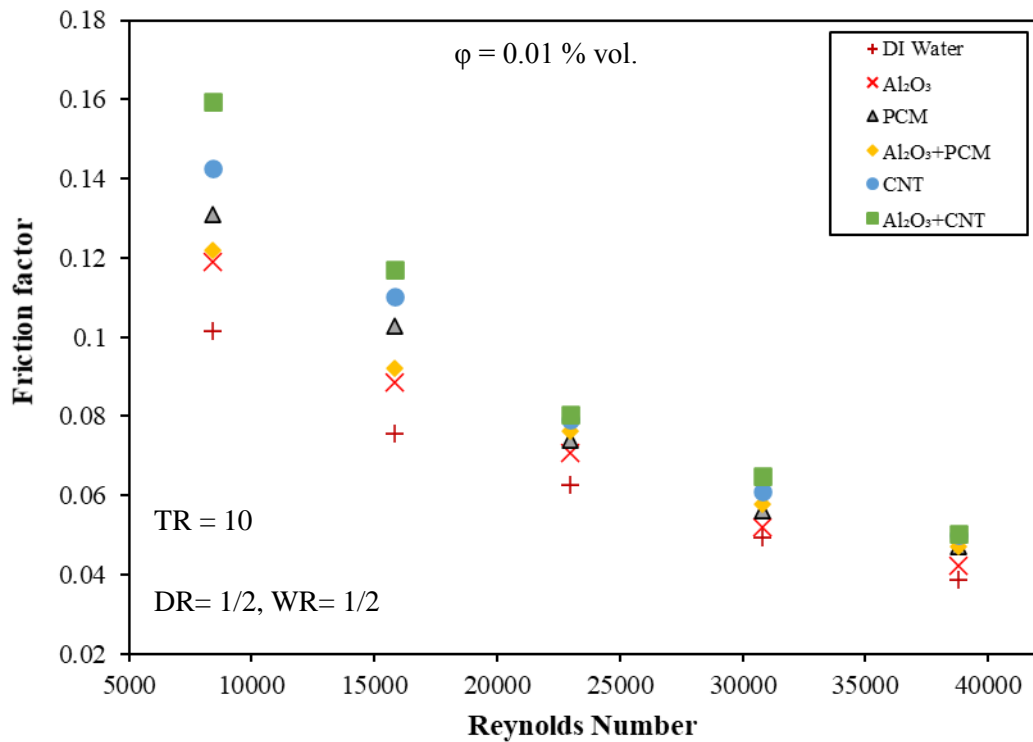


Figure 4.11. Variation of friction factor with nanofluid flow rate for different nanofluids

Figs. 4.12 and 4.13 show the variation of the ratio $h_i/\Delta p$ and entropy generation with respect to the nanofluid flow rate. As seen in Fig 4.12, the ratio $h_i/\Delta p$ decreases with an increase in the nanofluid flow rate for all cases of working fluids. The ratio $h_i/\Delta p$ yields maximum value at a low flow rate as h_i dominances over Δp at a low flow rate. Among all working fluids, Al_2O_3+CNT shows maximum $h_i/\Delta p$ value (4.56) at a low flow rate of 5 lpm. The $h/\Delta p$ ratio of Al_2O_3+CNT varies from 2.67 to 4.56. It is also observed that at the low flow rate, Al_2O_3 and Al_2O_3+PCM nanofluid have lower $h_i/\Delta p$ value than DI water irrespective of the increase in heat transfer coefficient, due to the fact that the pressure drop increment dominants over the heat transfer coefficient at a low flow rate. In Fig 4.13, the total entropy generation rises with an increase in the nanofluid flow rate. Adding of solid nanoparticles in the base fluid leads to decrease the effective temperature differences and increase the pressure drop and thus significantly decrease of total entropy generation. Also, the results show that the entropy generation of all working fluids is lesser than that of the DI water. Among all working fluids, Al_2O_3+PCM shows the minimum value of the entropy generation. This may be due to the combined effect of thermal irreversibility and pressure drop irreversibility. In comparison to DI water, using V-cut twisted tape of same twist ratio, $TR=10$ and same depth and width ratio ($DR=1/2$, $WR=1/2$), the average total entropy generation was reduced 14.74 % for Al_2O_3+PCM of 0.01 vol.% concentration hybrid nanofluid.

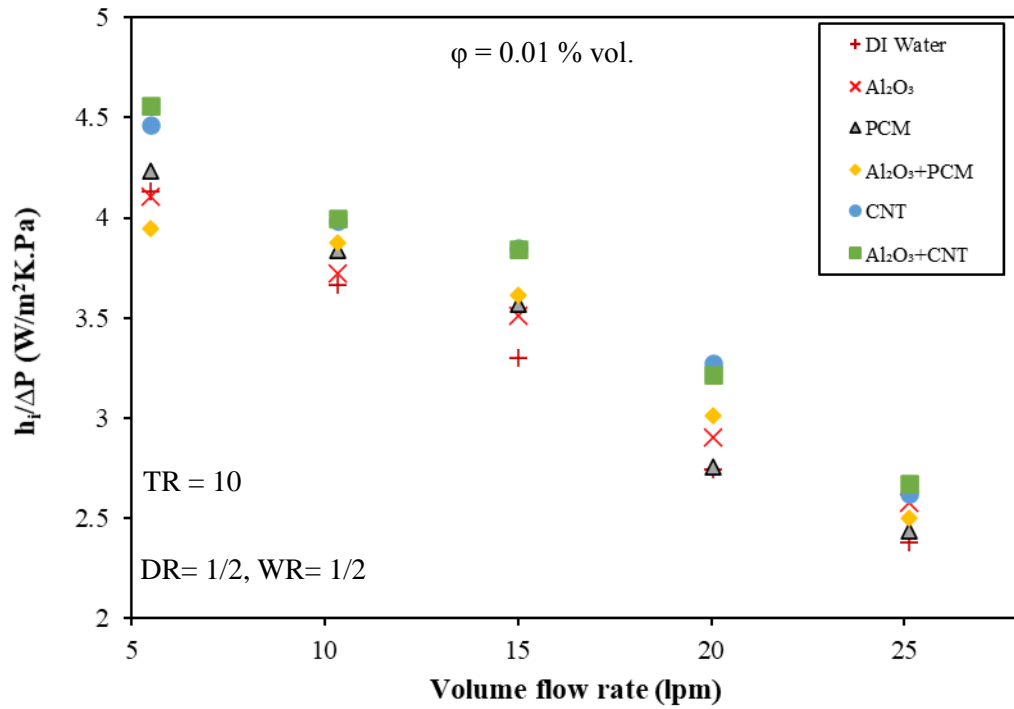


Figure 4.12. Variation of ratio $h_i/\Delta P$ with flow rate for different mono/hybrid nanofluids

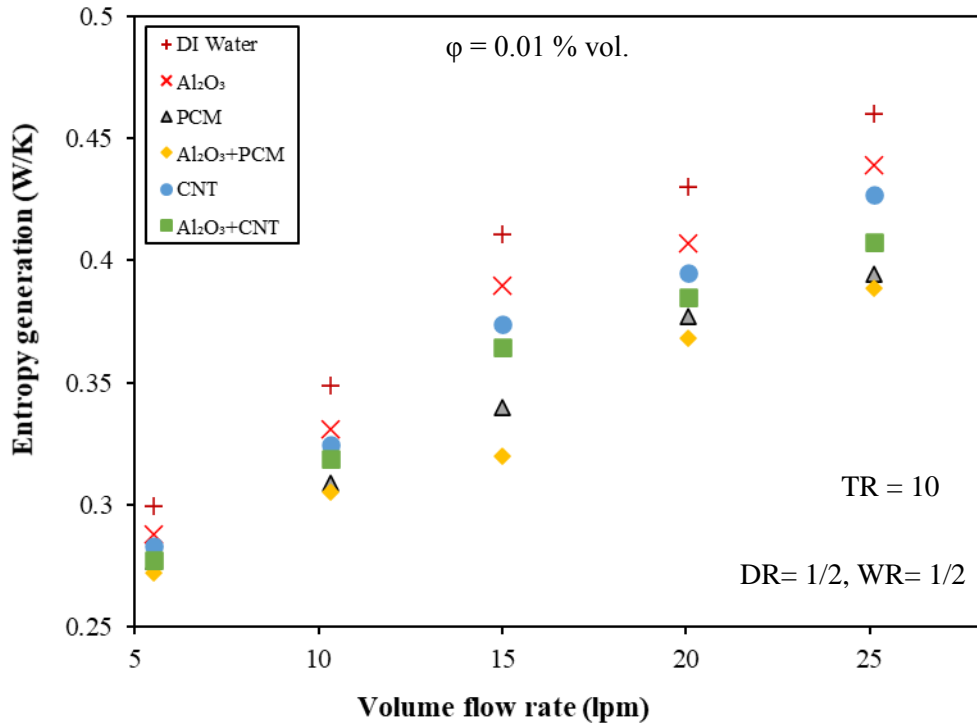


Figure 4.13. Variation of entropy generation with nanofluid flow rate for different nanofluids

4.4.1.2 Effect of volume concentration

Figs. 4.14 and 4.15 show the influence of volume concentration of nanofluid on the heat transfer coefficient (h_i) and pressure drop (Δp) with mean twist ratio ($TR=10$) and constant depth and width ratios ($DR=1/2$, $WR=1/2$). The results show that h_i and Δp are greater than those of the DI water and increase with an increase in volume concentration. With the addition of nanoparticles in the base fluid, it increases the thermal conductivity and fluid viscosity, which are the key factors for the enhancement of the heat transfer and pressure drop. Due to nanoparticles collision and the pseudoplastic behavior of the nanofluid, it enhances the thermal conductivity. The apparent viscosity of the nanofluid decreases due to the higher shear rate near the wall, which leads to diminishing the boundary layer and thus augments the heat transfer. The shear force, acting on the wall, increases due to the presence of nanoparticles, which cause an increase of pressure drop. The maximum value of h_i and Δp are observed 5392.5 W/m²K for Al₂O₃+PCM hybrid nanofluid and 2107.9 Pa for PCM, respectively, at a higher flow rate (25 lpm) and 0.1% volume concentration. When the volume concentration increases from 0.01 to 0.1%, the maximum augmentation of 11.46% in the heat transfer coefficient for Al₂O₃+PCM and 5.32% in pressure drop for PCM was found respectively at the flow rate of 25 lpm.

The comparisons of Nusselt number and friction factor with respect to Reynolds number for different volume concentrations (0.01% and 0.1%) using V-cuts twisted tape of same twist ratio and same depth and width ratio ($DR=1/2$ and $WR=1/2$) are illustrated in Figs. 4.16 and 4.17. The results reveal that with an increase in volume concentration from 0.01% to 0.1%, Nusselt number and friction factor also increases. When the volume concentration of mono/hybrid nanofluid increases, the thermal conductivity also increases, causing an enhancement in the heat transfer coefficient, which ultimately leads to a rise in the Nusselt number. The increase in friction factor is due to the rise in the viscosity of the

nanofluids when the nanoparticles are added in the base fluids. Al_2O_3 +PCM hybrid nanofluid of 0.1% volume concentration shows a higher Nusselt number and friction factor at high Reynolds number, while PCM nanofluid of 0.1% volume concentration shows high Nusselt number and friction factor at low Reynolds number. When the volume concentration increases from 0.01 to 0.1%, the average enhancement of Nu is 11.11 % for Al_2O_3 +PCM, 16.86 % for Al_2O_3 and 15.25 % for PCM, while the average enhancement of friction factor is 11.24% for Al_2O_3 +PCM, 10.60 % for PCM, and 6.86% for Al_2O_3 respectively, for the same twist ratio and same depth and width ratios (DR=1/2, WR=1/2).

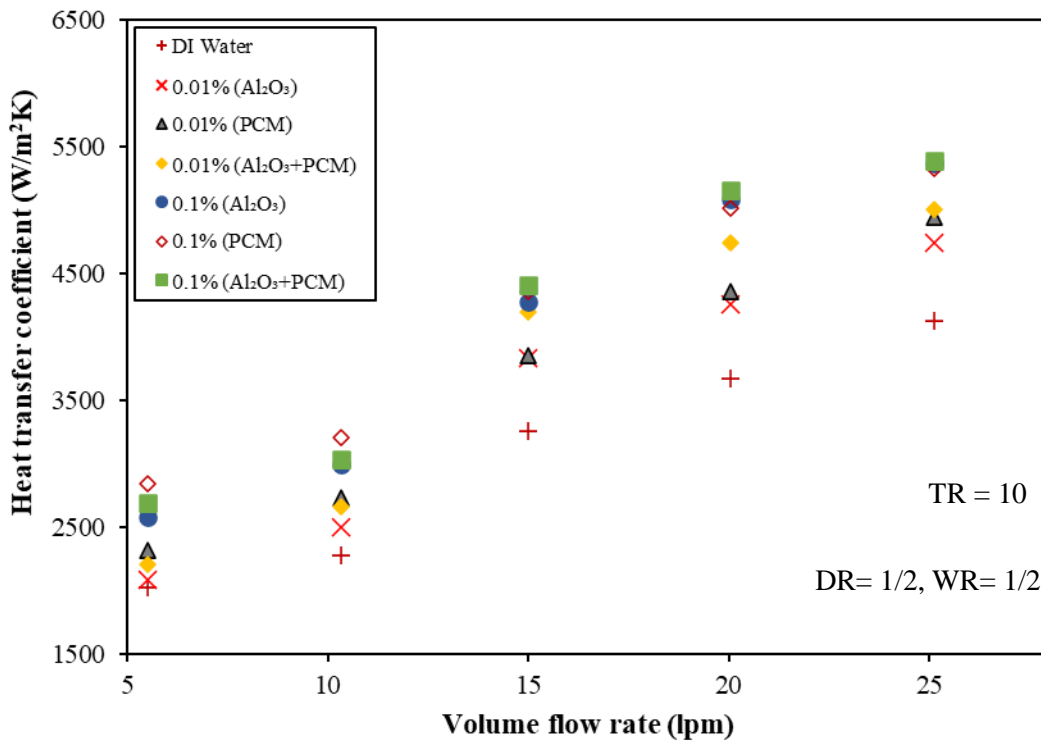


Figure 4.14. Variation of heat transfer coefficient with flow rate for different concentrations

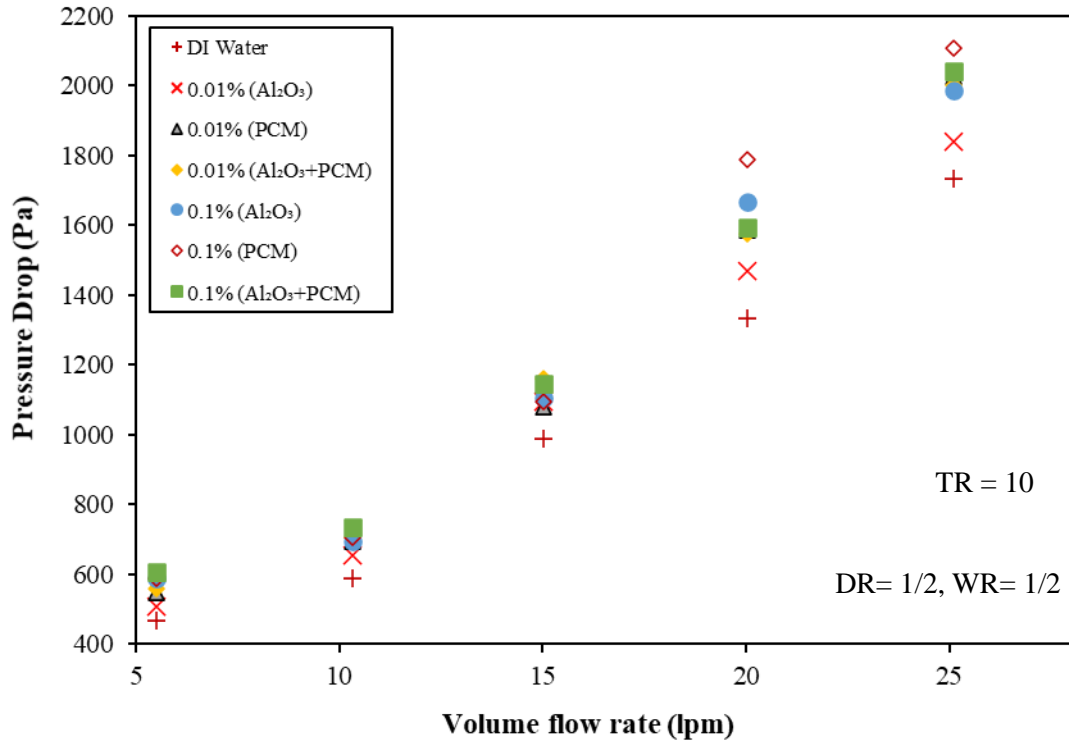


Figure 4.15. Variation of pressure drop with nanofluid flow rate for different concentrations

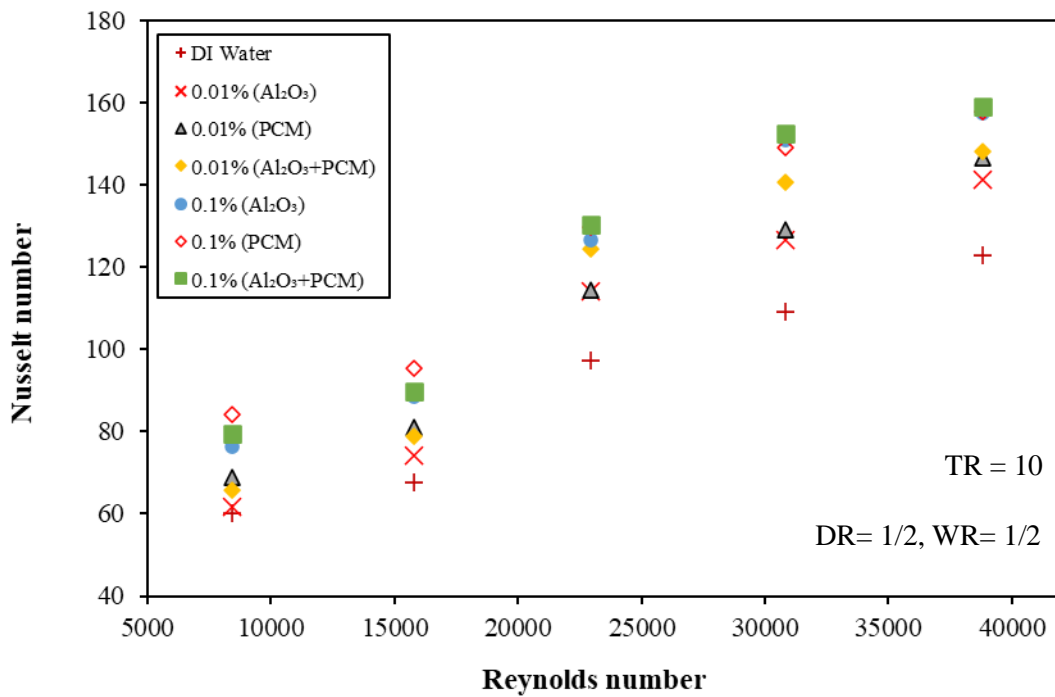


Figure 4.16. Variation of Nusselt number with Reynolds number for different concentrations

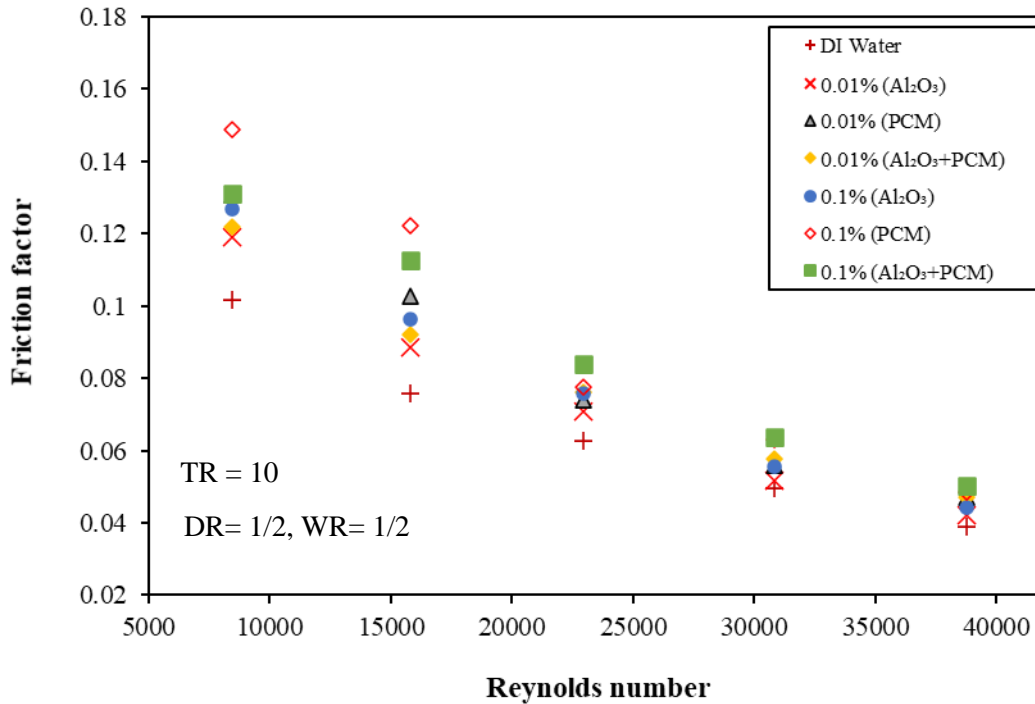


Figure 4.17. Variation of friction factor with Reynolds number for different concentrations

Figs. 4.18 and 4.19 show the variation of the ratio $h_i/\Delta p$ and entropy generation with respect to the nanofluid flow rate. As seen in Fig 4.18, the ratio $h_i/\Delta p$ decreases with an increase in the nanofluid flow rate for all cases of working fluids. Also, all working fluids of 0.1 vol.% concentration have higher $h_i/\Delta p$ value than working fluids of 0.01 vol.% concentration. Among all working fluids, PCM shows maximum $h_i/\Delta p$ value at a low flow rate of 5 lpm. It is also observed that at a low flow rate, Al₂O₃ and Al₂O₃+PCM of 0.01 vol.% concentration nanofluid have lower $h_i/\Delta p$ value than DI water irrespective of the increase in heat transfer coefficient, due to the fact that the pressure drop increment dominates over the heat transfer coefficient at a low flow rate. In Fig 4.19, with an increase in volume concentration from 0.01 to 0.1%, the entropy generation decreases. This is because an increase in volume concentration leads to improve heat transfer performance and hence less irreversibilities due to heat transfer. Adding of solid nanoparticles in the base fluid leads to decrease the effective temperature differences and increase the pressure drop and thus

significantly decrease of total entropy generation. Also, the results show that the entropy generation of all working fluids is lesser than that of the DI water. When the volume concentration increased from 0.01% to 0.1%, the average total entropy generation was reduced by about 11.94 % for Al_2O_3 +PCM using V-cut twisted tape of the same twist ratio, $\text{TR}=10$ and same depth and width ratio ($\text{DR}=1/2$, $\text{WR}=1/2$).

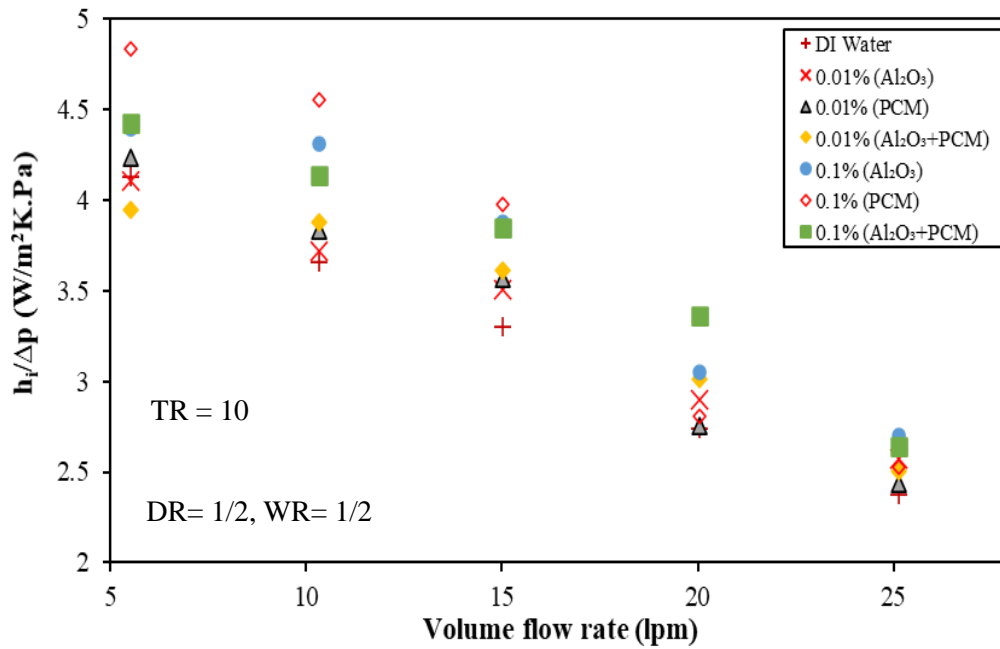


Figure 4.18. Variation of ratio $h_i/\Delta p$ with nanofluid flow rate for different volume concentration

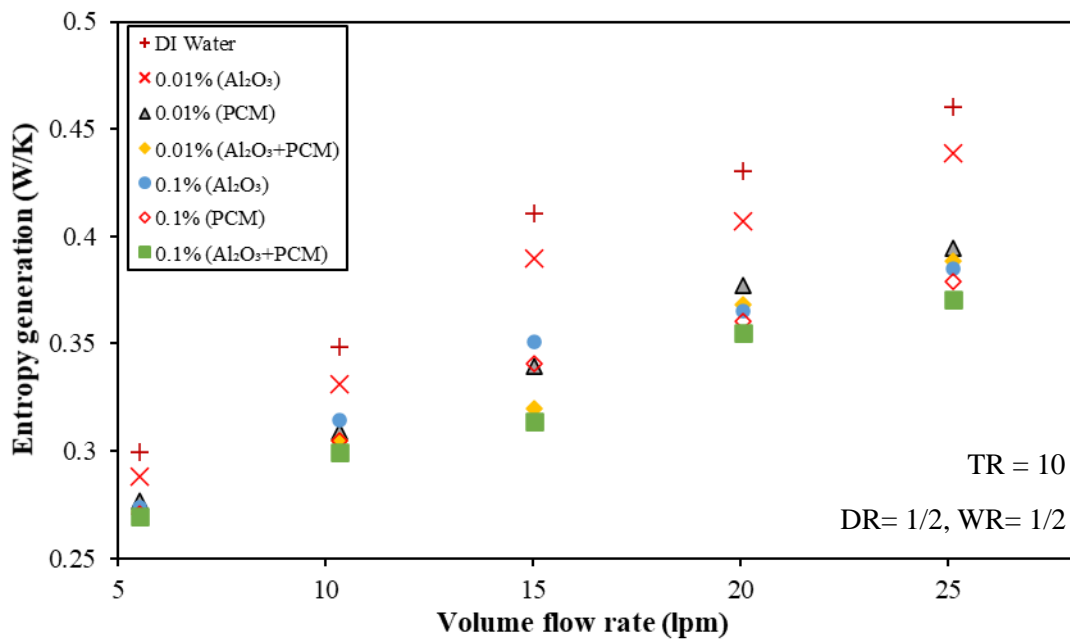


Figure 4.19. Variation of entropy generation with flow rate for different concentrations

4.4.1.3 Effect of twist ratio

Figs. 4.20 and 4.21 demonstrate the effects of twist ratio of the V-cut twisted tape inserts on the heat transfer characteristics and pressure drop for the same volume concentration ($\phi = 0.01\%$), same volume flow rate (15 lpm) and same depth and width ratio ($DR=1/2$, $WR=1/2$). The results reveal that heat transfer characteristics (h_i) and pressure drop (Δp) increase with decreasing the twist ratio. This can be explained that with decreasing the twist ratio, it raises the swirl flow, which creates a better mixing of the fluid. This swirl flow diminishes the boundary layer thickness and increases flow turbulence intensity, which leads to greater heat transfer along with the penalty of pressure drop. The insertions of the twisted tapes of a lower twist ratio in a tube induce high swirl motion into the core flow, which creates more disturbance near the wall. For $TR = 5$, the maximum value of h_i is observed 6049.6 W/m^2K for Al_2O_3+CNT followed by CNT (5858 W/m^2K), Al_2O_3+PCM (5344.2 W/m^2K), Al_2O_3 (4447.9 W/m^2K) and PCM (4447.7 W/m^2K) hybrid nanofluid and the maximum value of Δp is observed 1360.8 Pa for Al_2O_3+CNT followed by CNT (1320.8 Pa), Al_2O_3+PCM (1240.7 Pa), Al_2O_3 (1120.6 Pa) and PCM (1107.3 Pa) hybrid nanofluid respectively. For Al_2O_3+CNT hybrid nanofluid and $TR = 5$, the average higher h_i and Δp are 63.62% and 30.76%, respectively, greater than that of DI water as the working fluid.

Figs. 4.22 and 4.23 show the impact of using V-cut twisted tapes on the Nusselt number and friction factor with different twist ratios for the same volume concentration ($\phi = 0.01\%$), same volume flow rate (15 lpm) and same depth and width ratio ($DR=1/2$, $WR=1/2$). The results reveal that with decreasing the twist ratio (TR), both the Nusselt number and friction factor increases. The reason is that with decreasing the twist ratio, it raises the swirl flow, which creates a better mixing of the fluid, as mentioned earlier. This swirl flow diminishes the boundary layer thickness and increases flow turbulence intensity, which leads to greater heat transfer. The centrifugal forces originated by the swirling motion impinge over

the wall, which leads to higher heat transfer. For Al_2O_3 +PCM hybrid nanofluid, the Nusselt number for TR=5 is enhanced by 27.38% greater than that for TR=10 and 41.03 % greater than that for TR= 15 while, the friction factor for TR = 5, is enhanced by 3.39 % greater than that for TR =10 and 25.55 % greater than that for TR=15, respectively for the same depth and width ratios (DR=1/2, WR=1/2) and volume flow rate of 15 lpm.

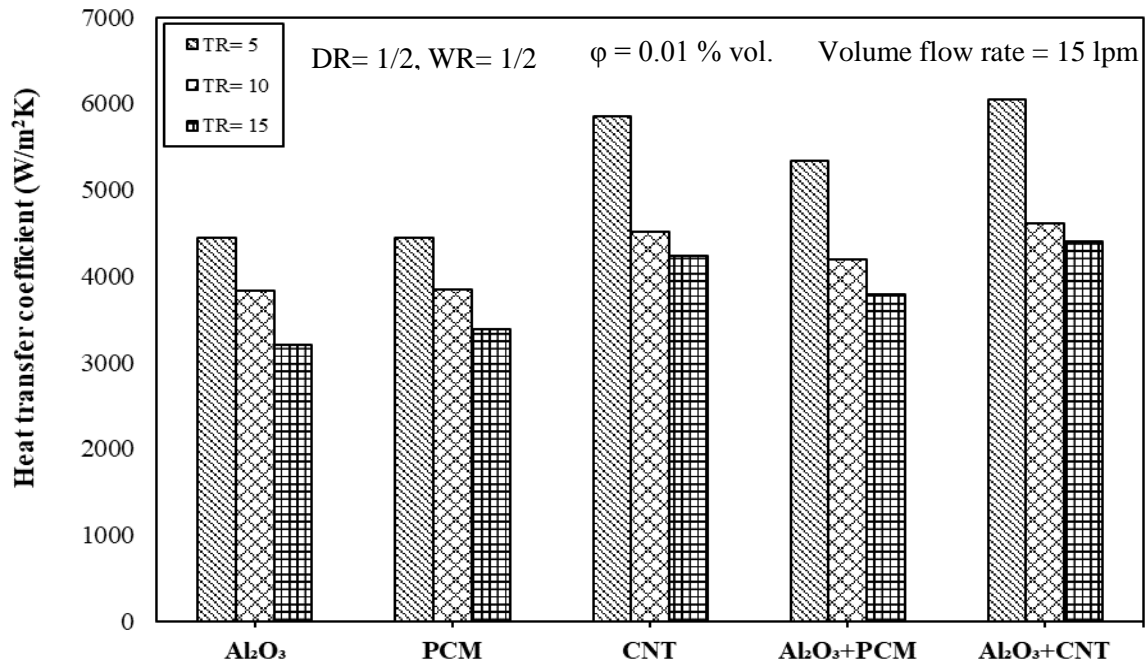


Figure 4.20. Variation of heat transfer coefficient with different nanofluids for different TR

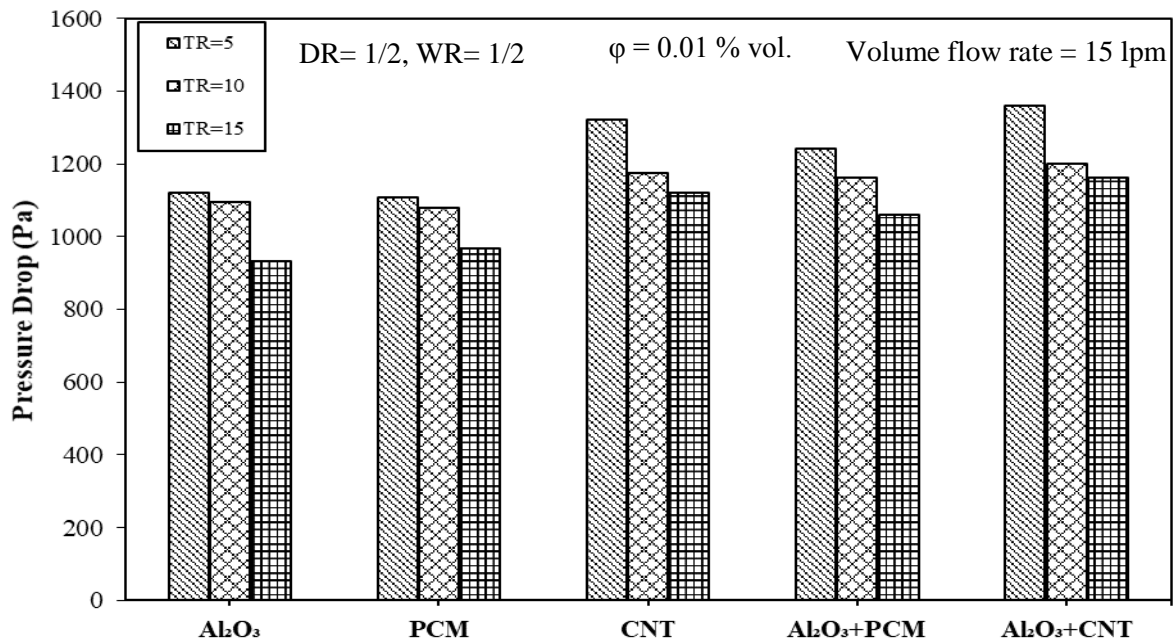


Figure 4.21. Variation of pressure drop with different mono/hybrid nanofluids for different TR

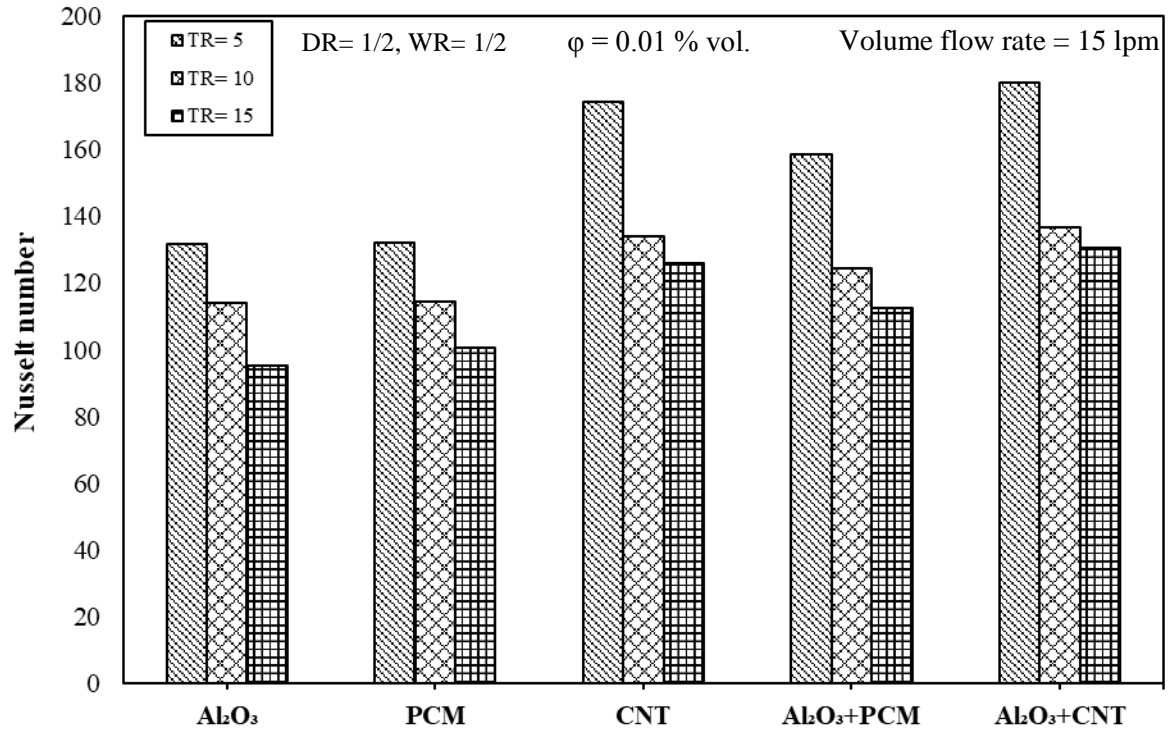


Figure 4.22. Variation of Nusselt number with different mono/hybrid nanofluid for different

TR

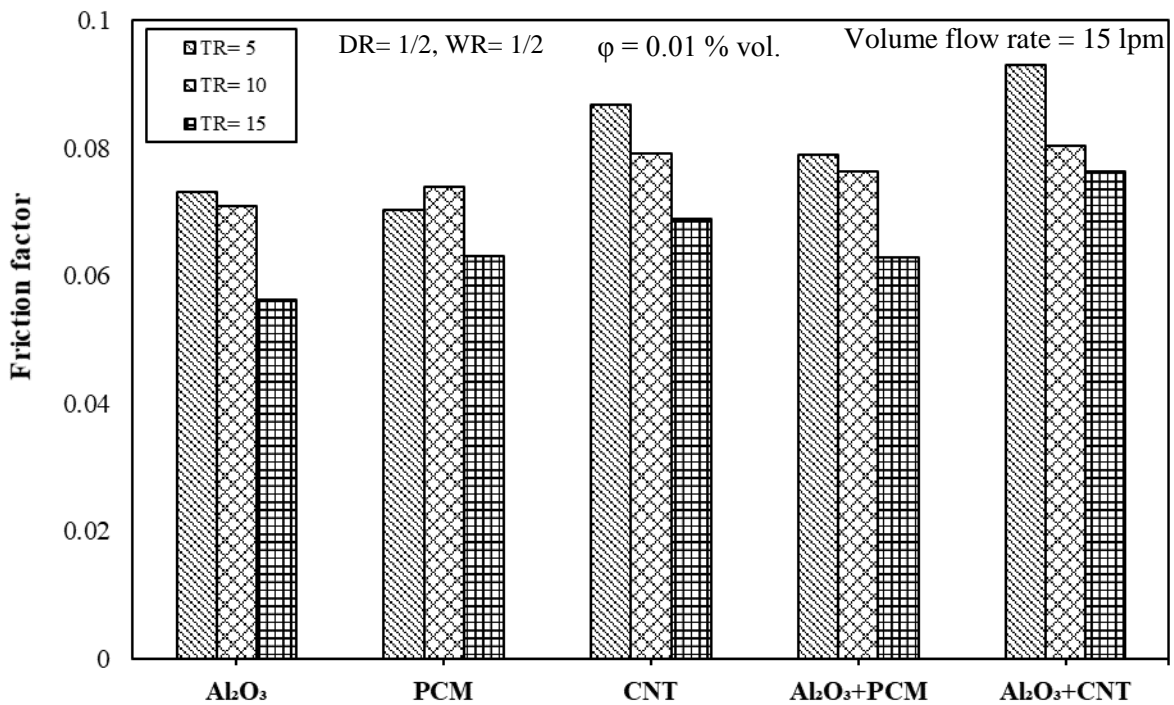


Figure 4.23. Variation of friction factor with different mono/hybrid nanofluid for different

TR

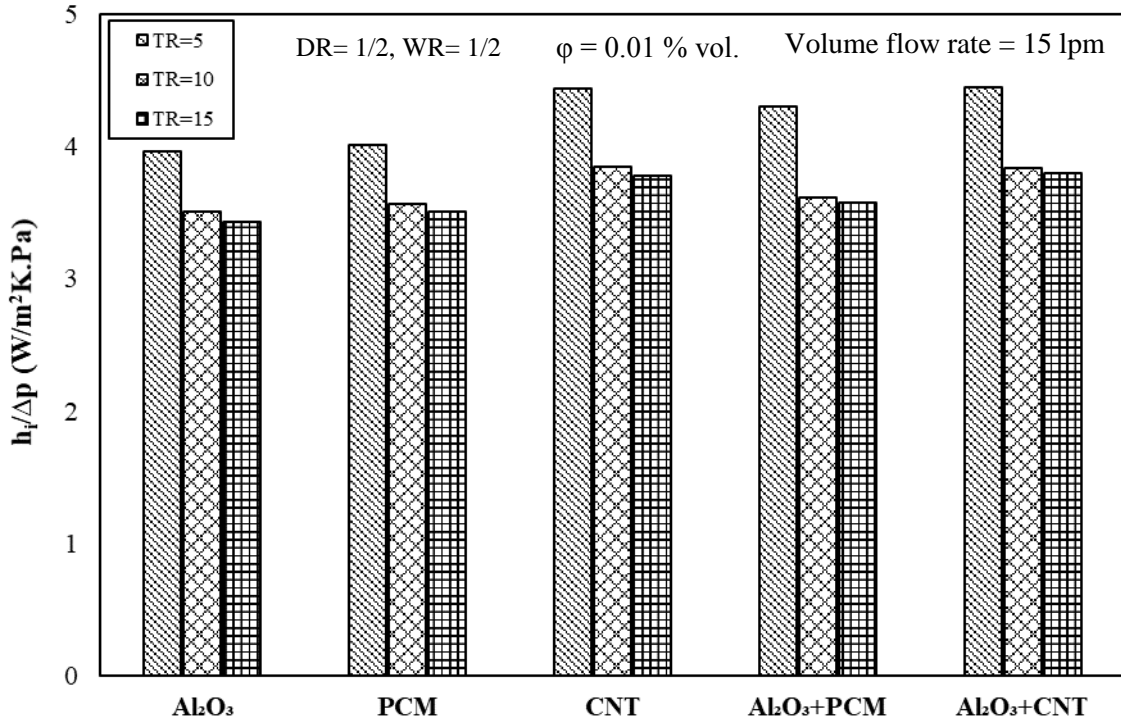


Figure 4.24. Variation of $h_i/\Delta p$ with different mono and hybrid nanofluid for different TR

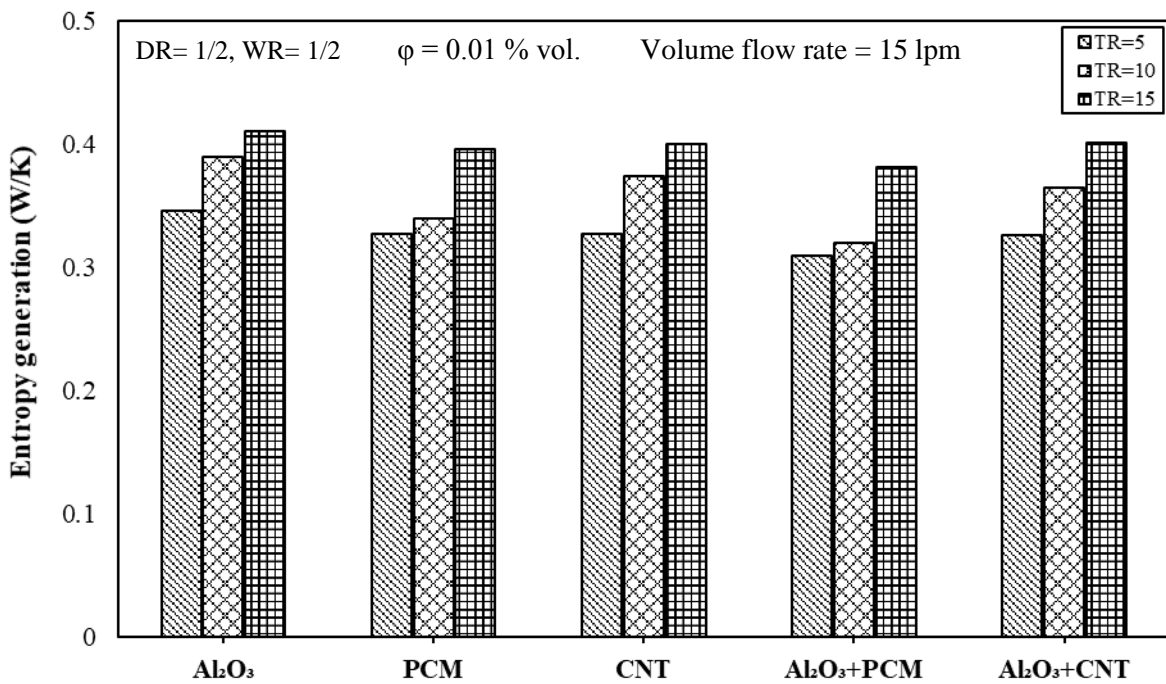


Figure 4.25. Variation of entropy generation with different nanofluid for different TR

Figs. 4.24 and 4.25 show the variation of the ratio $h_i/\Delta p$ and entropy generation with respect to different mono and hybrid nanofluid for different twist ratio at the same volume concentration ($\phi = 0.01\%$), same volume flow rate (15 lpm) and depth and width ratio ($DR=1/2$, $WR=1/2$). The results reveal that, with an increase in twist ratio, the ratio $h_i/\Delta p$ decreases. This is because, at a low twist ratio, the heat transfer coefficient dominates and at a high twist ratio, pressure drop dominates. The ratio $h_i/\Delta p$ shows the maximum value for Al_2O_3+CNT using V-cuts twisted tape of $TR=5$. It is due to the fact that for the same twist ratio, the increment in h_i dominates over the Δp . Al_2O_3 shows the minimum value of $h_i/\Delta p$ for $TR=5$ among all working fluid, as an increment in pressure drop dominates over the heat transfer coefficient. In Fig 4.25, the total entropy generation rises with an increase in twist ratio for all working fluids. This is due to the fact that a lower twist ratio creates a strong mixing of fluids, which in results improves heat transfer and reduces the value of entropy generation. Using V-cut twisted tape of $TR=15$, Al_2O_3 shows maximum entropy generation while Al_2O_3+PCM shows minimum entropy generation when V-cut twisted tape of $TR=5$ is used. In comparison to $TR=15$ using Al_2O_3+PCM hybrid nanofluid, using V-cut twisted tape of the same depth and width ratio ($DR=1/2$, $WR=1/2$), the result found 18.79 % reduction in total entropy generation for $TR=5$ of and 16.12% for $TR=10$ respectively.

4.4.1.4 Effects of depth and width ratios

Figs. 4.26 and 4.27 show the effect of depth and width ratio of V-cuts twisted tape on the heat transfer coefficient and pressure for the different mono and hybrid nanofluid at the same volume concentration ($\phi = 0.01\%$), volume flow rate (15 lpm) and mean twist ratio, $TR=10$. The results reveal that h_i and Δp increase with an increase in depth ratio and decrease in width ratio in the case of all working fluids. The reason for this enhancement is that for higher DR and lower WR , the vorticity behind the cuts is more developed extra turbulence and enhancing the heat transfer rate with the penalty of Δp . The synergy of vortex circulation,

together with secondary flow, increases the turbulence near the heated surface of the tube. For $DR=1/2$, $WR=1/3$, the maximum value of heat transfer coefficient is observed 5118.3 W/m^2K for Al_2O_3+CNT followed by CNT (5020.1 W/m^2K), Al_2O_3+PCM (4733.7 W/m^2K), PCM (4075.7 W/m^2K) and Al_2O_3 (3974.7 W/m^2K) hybrid nanofluid and the maximum value of pressure drop is observed 1227.4 Pa for Al_2O_3+CNT followed by CNT (1214 Pa), Al_2O_3+PCM (1174 Pa), Al_2O_3 (1107.3 Pa) and PCM (1094 Pa) hybrid nanofluid respectively. The maximum enhancement of h_i and Δp for V-cuts twisted tape of $DR=1/2$ and $WR=1/3$ are around 12.36 % is found for Al_2O_3+PCM hybrid nanofluid, and 3.65 % for PCM hybrid nanofluid, respectively, when compared to V-cuts twisted tape of $DR=1/3$ and $WR=1/2$ at the same flow of 15 lpm. It can be concluded that higher depth ratio, i.e., $DR=1/2$ and lower width ratio, i.e., $WR=1/3$ enhanced higher heat transfer rate with the penalty of Δp than those V-cuts twisted tape with lower depth ratio, i.e., $DR=1/3$ and higher width ratio, i.e., $WR=1/2$.

Figs. 4.28 and 4.29 demonstrate the effect of depth and width ratio of V-cuts twisted tape on the Nusselt number and friction factor for the different mono and hybrid nanofluid at the same volume concentration ($\phi = 0.01\%$), volume flow rate (15 lpm) and mean twist ratio, $TR=10$. The results reveal that the Nusselt number and friction factor increase with the increase in depth ratio and decrease in width ratio. Al_2O_3+CNT /water shows a higher Nusselt number and friction factor among all working fluids using V-cut twisted tape of the same depth and width ratios. Nusselt number and friction factor of Al_2O_3+PCM hybrid nanofluid using V-cuts twisted tape of $DR=1/2$ and $WR=1/3$ are enhanced by around 13.96% and 3.72%, respectively, when compared to V-cuts twisted tape of $DR=1/3$ and $WR=1/2$ at the volume flow rate of 15 lpm.

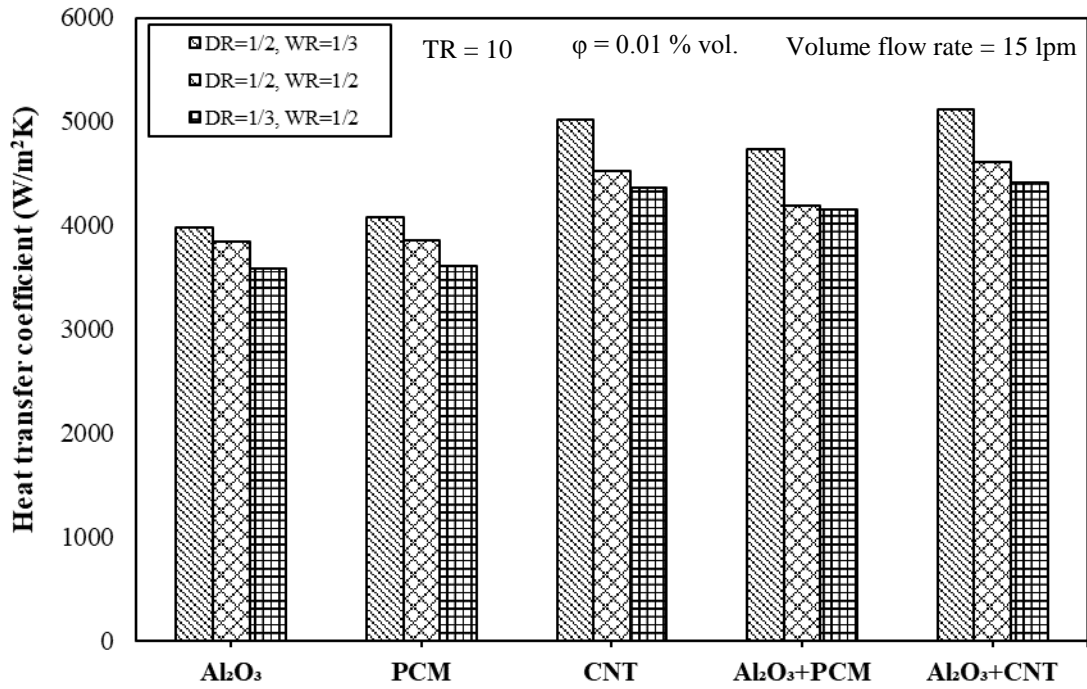


Figure 4.26. Variation of heat transfer coefficient for different nanofluid, DR and WR

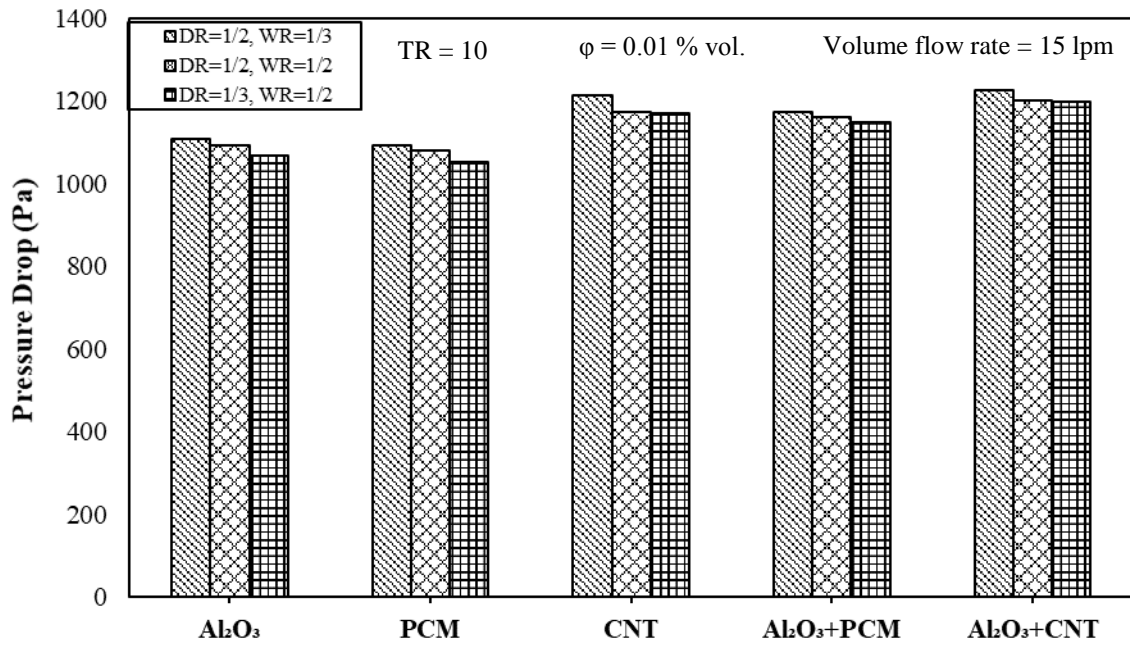


Figure 4.27. Variation of pressure drop with different nanofluid, DR and WR

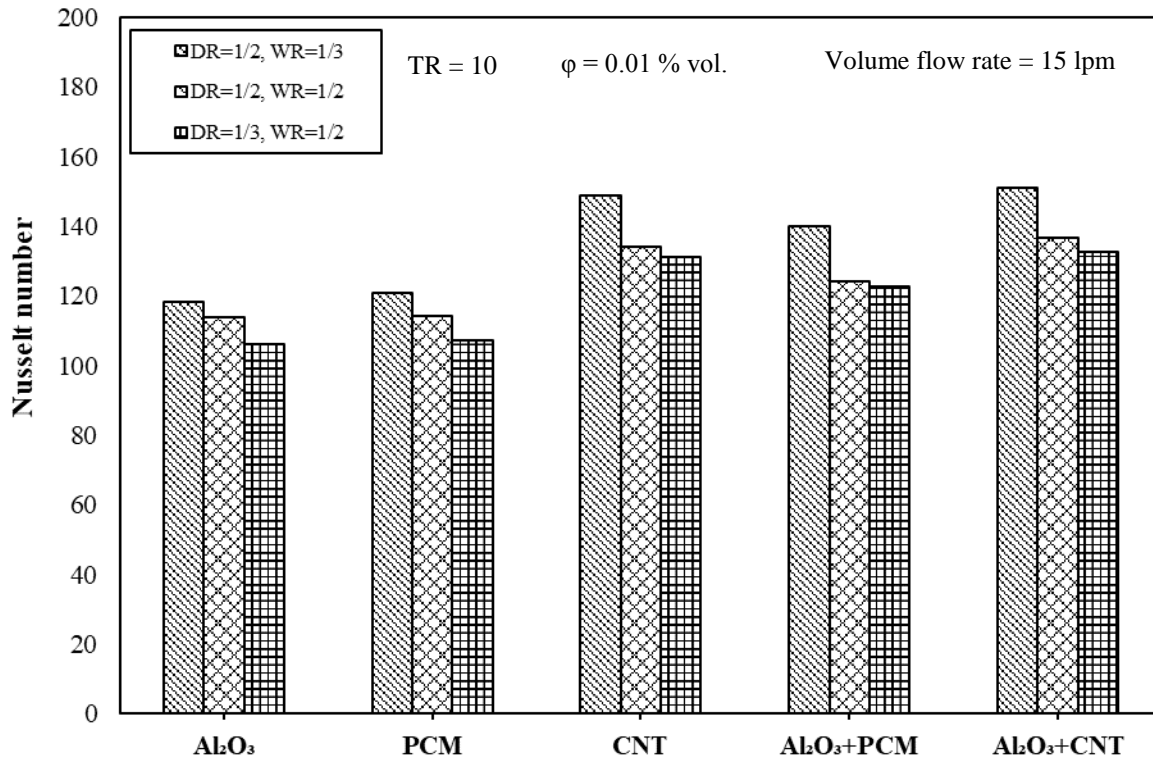


Figure 4.28. Variation of Nusselt number with different mono/hybrid nanofluid, DR and WR

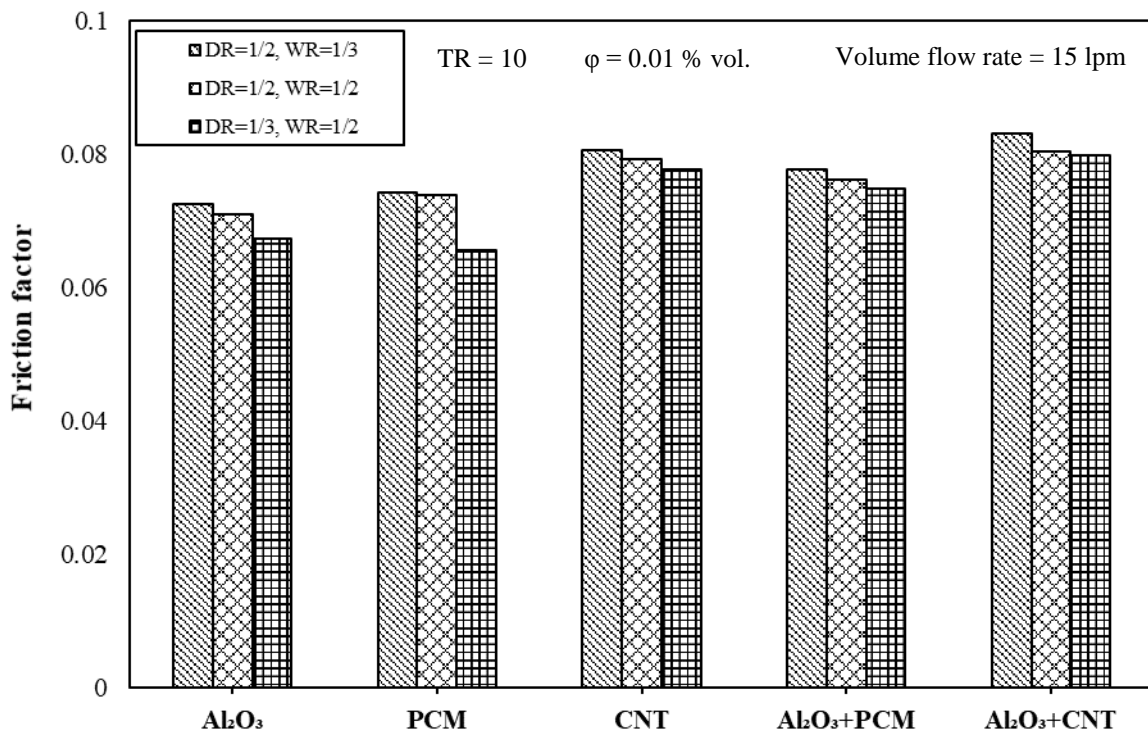


Figure 4.29. Variation of friction factor with different mono/hybrid nanofluid, DR and WR

Figs. 4.30 and 4.31 show the variation of the ratio $h_i/\Delta p$ and entropy generation with respect to different mono and hybrid nanofluid at the same volume concentration ($\phi = 0.01\%$), volume flow rate (15 lpm) and mean twist ratio, $TR=10$. The ratio $h_i/\Delta p$ shows the maximum value for Al_2O_3+CNT using V-cuts twisted tape of $DR=1/2$, $WR=1/3$ among all working fluids. With the V-cuts twisted tape of $DR=1/2$, $WR=1/3$, the ratio $h_i/\Delta p$ exhibits higher value than that of V-cuts twisted tape of $DR=1/3$, $WR=1/2$ as the pressure drop is low at the same flow rate. In Fig 4.31, the total entropy generation increases with a decrease in DR and an increase in WR for all working fluids. Using V-cut twisted tape of $DR=1/3$, $WR=1/2$, Al_2O_3 shows maximum entropy generation while Al_2O_3+PCM shows minimum entropy generation when V-cut twisted tape of $DR=1/2$, $WR=1/3$ is used. In comparison to $DR=1/3$, $WR=1/2$ using Al_2O_3+PCM hybrid nanofluid, using V-cut twisted tape of same twist ratio $TR=10$, the result observed 13.29 % reduction in total entropy generation for $DR=1/2$, $WR=1/3$.

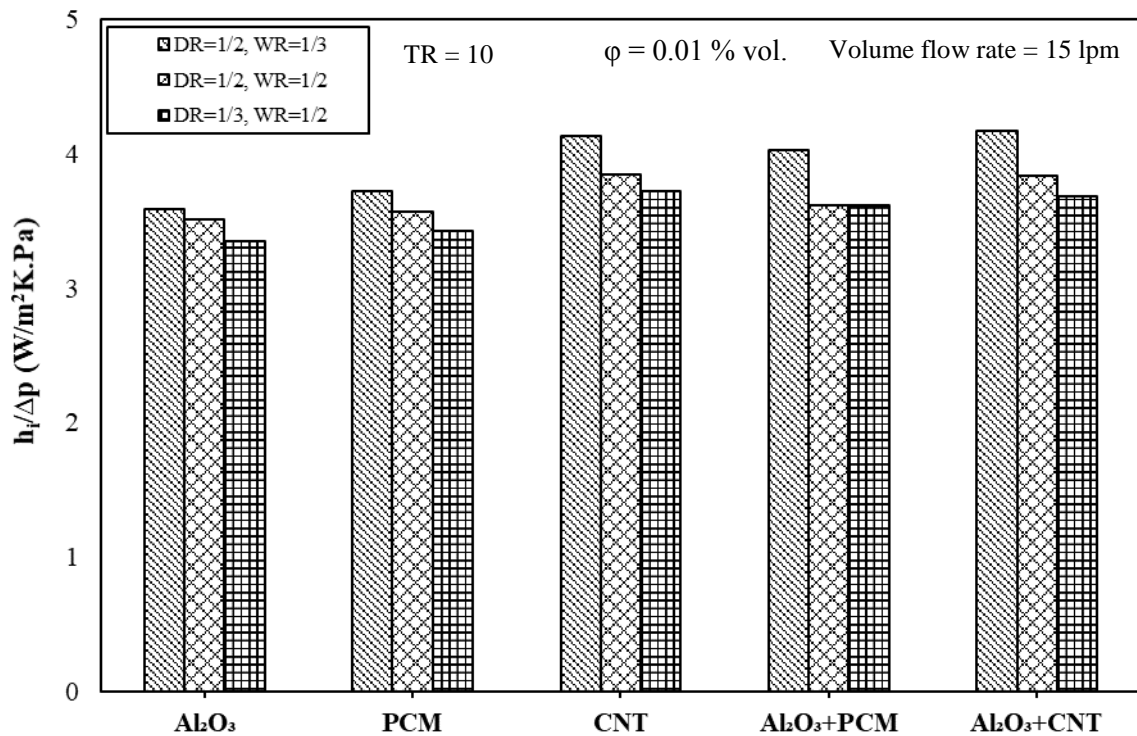


Figure 4.30. Variation of $h_i/\Delta p$ with different mono/hybrid nanofluid, DR and WR

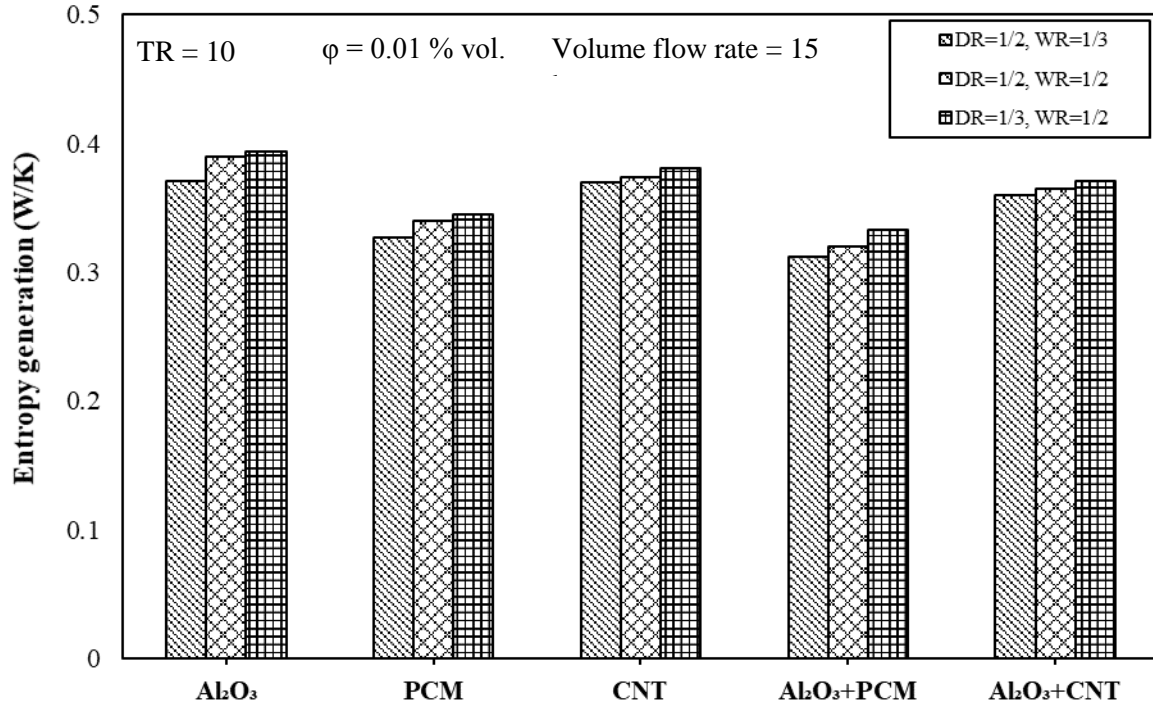


Figure 4.31. Variation of entropy generation with different mono/hybrid nanofluid, DR and WR

4.4.1.5 Effect of nanofluid inlet temperature

Figs. 4.32 and 4.33 illustrate the effect of nanofluid volume flow rate on heat transfer coefficient and pressure drop with a different inlet temperature of 50°C, 60°C and 70°C for the same twisting ratio (TR=10) and same depth and width ratio (DR=1/2, WR=1/2). The results reveal that decreasing the inlet temperature of the hot fluid increases both the heat transfer coefficient and pressure drop. When the inlet temperature decreases, the temperature difference increases, which tends to increase the heat transfer rate for the same volume flow rate. Whereas the pressure drop in the tube also decreases with an increase in inlet temperature due to a decrease in fluid viscosity with nanofluid inlet temperature. At 50°C, the heat transfer coefficient of the hybrid nanofluid enhances by around 6.55 % than that of the base fluid and 14.80 % than that of hybrid nanofluid at 70°C, respectively, at the volume flow rate of 15 lpm. Whereas, at the inlet temperature of 50°C and volume flow rate of 15 lpm, the

pressure drop of the hybrid nanofluid enhances by around 2.56 % as compared to base fluid and is 4.16 % higher than that of hybrid nanofluid at 70°C.

The variation of Nusselt number and friction factor with respect to Reynolds number with different inlet temperatures of 50°C, 60°C and 70°C for the same twisting ratio (TR=10) and same depth and width ratio (DR=1/2, WR=1/2) are shown in Figs. 4.34 and 4.35. The results reveal that the Nusselt number and friction factor increase with decreasing the inlet temperature of hot fluid. The Nusselt number increases with a decrease in inlet temperature because of the similar trend of the heat transfer coefficient. At the same time, the friction factor in the pipe also decreases with an increase in inlet temperature as fluid viscosity decreases with an increase in inlet temperature. At 50°C, the Nusselt number of the hybrid nanofluid enhances around 9.24 % greater than that of the base fluid and 13.57 % more than that of hybrid nanofluid at 70°C, respectively. While on the other hand, at 50°C, the friction factor of the hybrid nanofluid enhances around 2.19 % higher than that of the base fluid and 8.74 % greater than that of hybrid nanofluid at 70°C respectively.

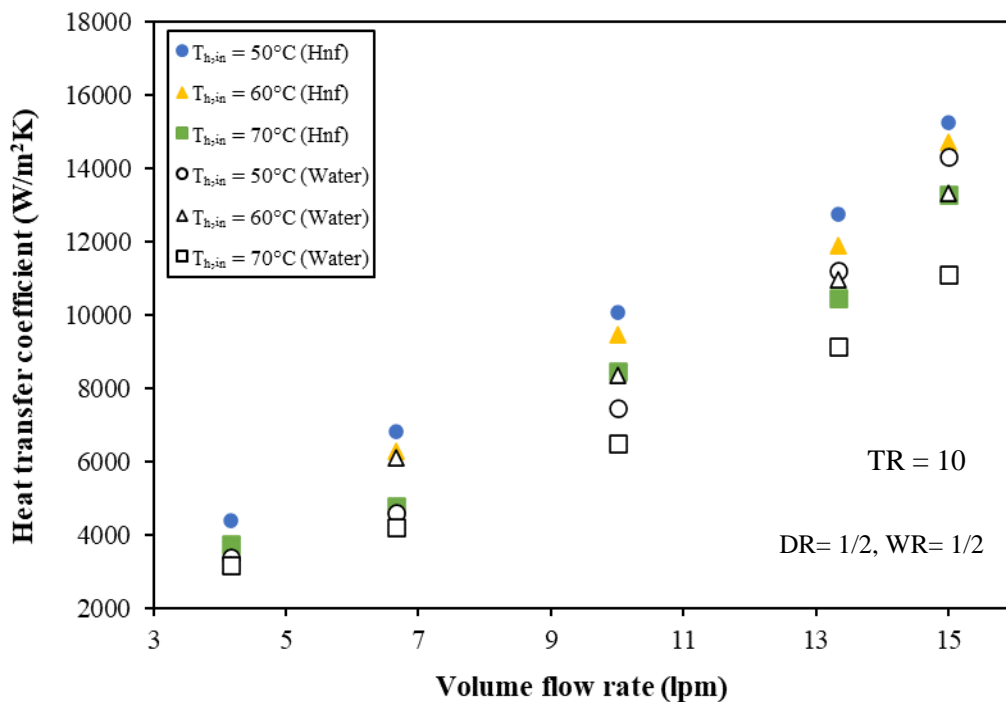


Figure 4.32. Variation of heat transfer coefficient with flow rate for different inlet temperatures

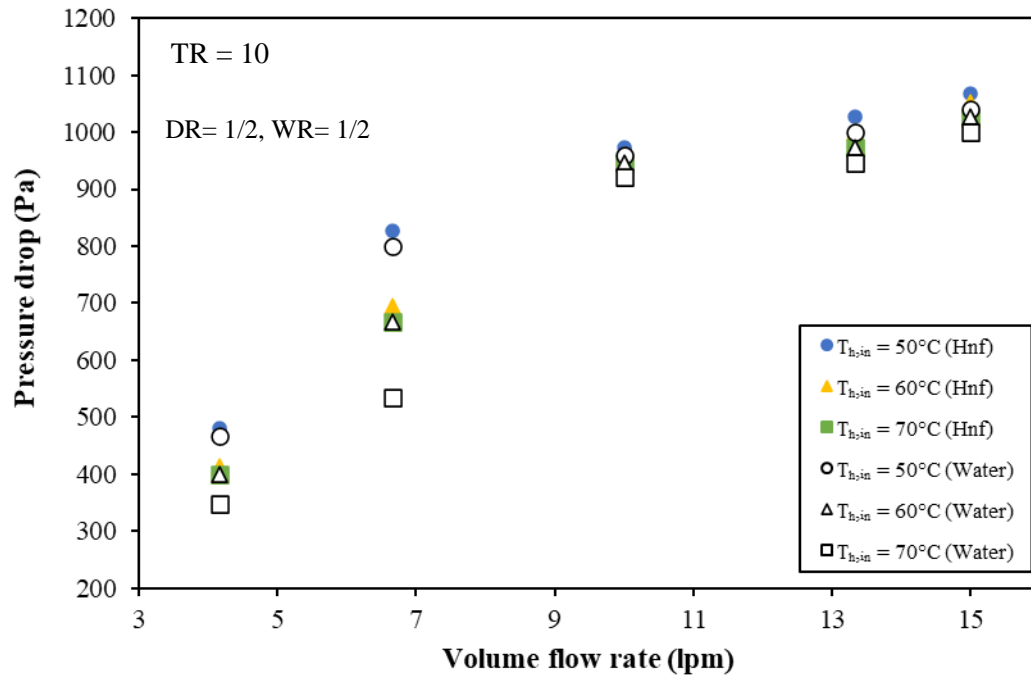


Figure 4.33. Variation of Pressure drop with nanofluid flow rate for different inlet temperatures

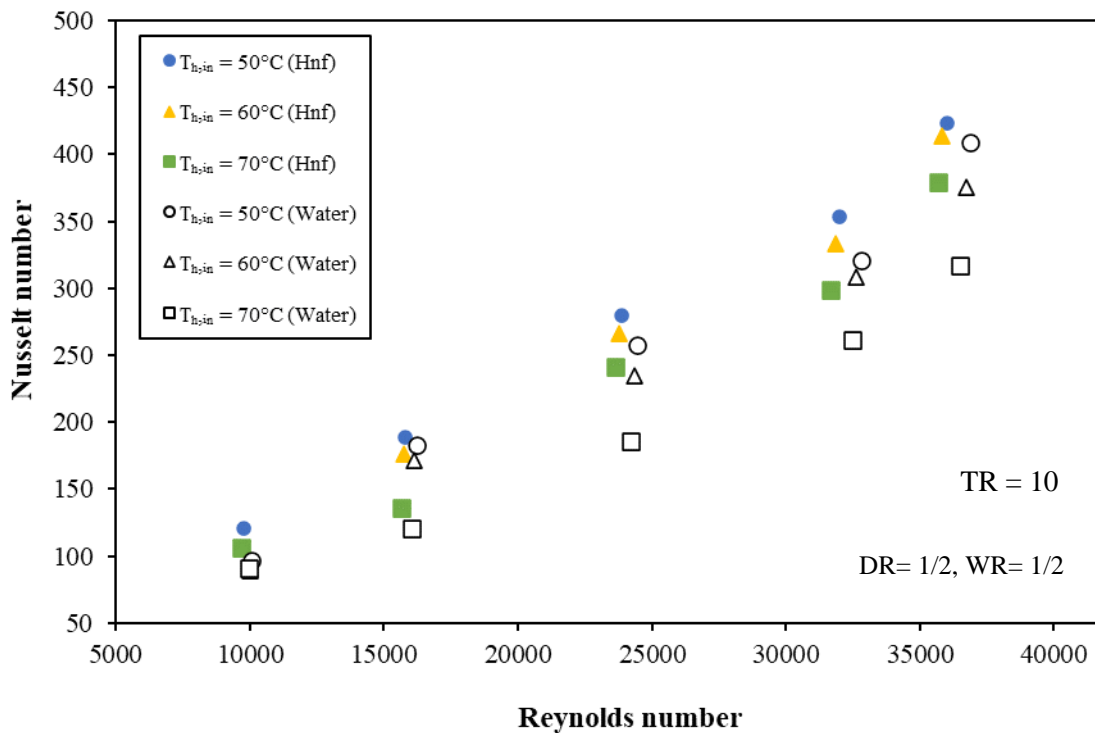


Figure 4.34. Variation of Nusselt number with Reynolds number for different inlet temperatures

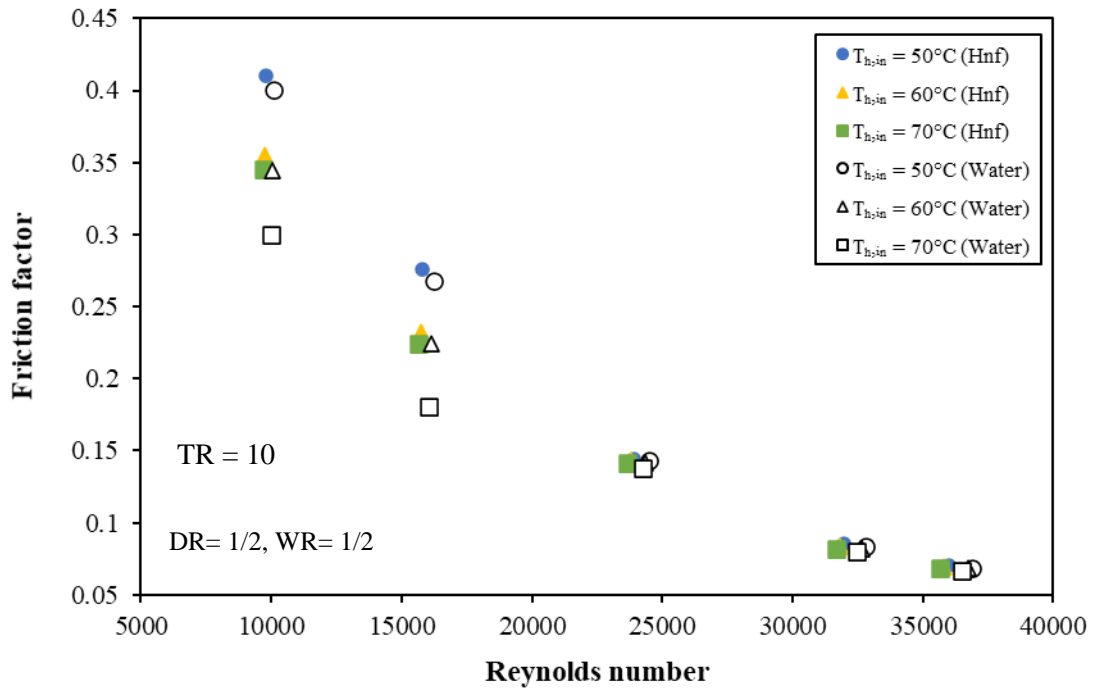


Figure 4.35. Variation of friction factor with Reynolds number for different inlet temperatures

Fig 4.36 and 4.37 presents the effect of the inlet temperature of hot hybrid nanofluid on the ratio $h_i/\Delta p$ and entropy generation with respect to nanofluid flow rate for the same twisting ratio, $TR= 10$ and same depth and width ratio ($DR=1/2$, $WR=1/2$). Values of ratio $h_i/\Delta p$ are greater than unity for hybrid nanofluid for all cases, which indicate that using hybrid nanofluid and V-cuts twisted tape inserts can be considered a better choice in practical application. From this figure, it is seen that the ratio $h_i/\Delta p$ decreases with an increase in the inlet temperature of hot nanofluid for the high nanofluid flow rate. At the high flow rate of 15 lpm, the ratio $h_i/\Delta p$ for V-cuts twisted tapes of twist ratio, $TR= 10$ and depth and width ratio ($DR=1/2$, $WR=1/2$) at 50°C is 3.89 % higher than that of the base fluid and 10.21 % higher than that of hybrid nanofluid at 70°C respectively. From Fig 4.37, it is seen that the entropy generation increases with an increase in the inlet temperature of hot nanofluid for the same nanofluid volume flow rate. This is due to the fact that with an increase in temperature, the fluid viscosity decreases, which leads to a decrease in fluid friction, which has a slight effect

on total entropy generation. At the high flow rate of 15 lpm, the entropy generation for V-cuts twisted tapes of TR = 10, DR=1/2 and WR=1/2 at 50°C is 6.41 % lower than that of the base fluid and 42.02 % lower than that of hybrid nanofluid at 70°C, respectively.

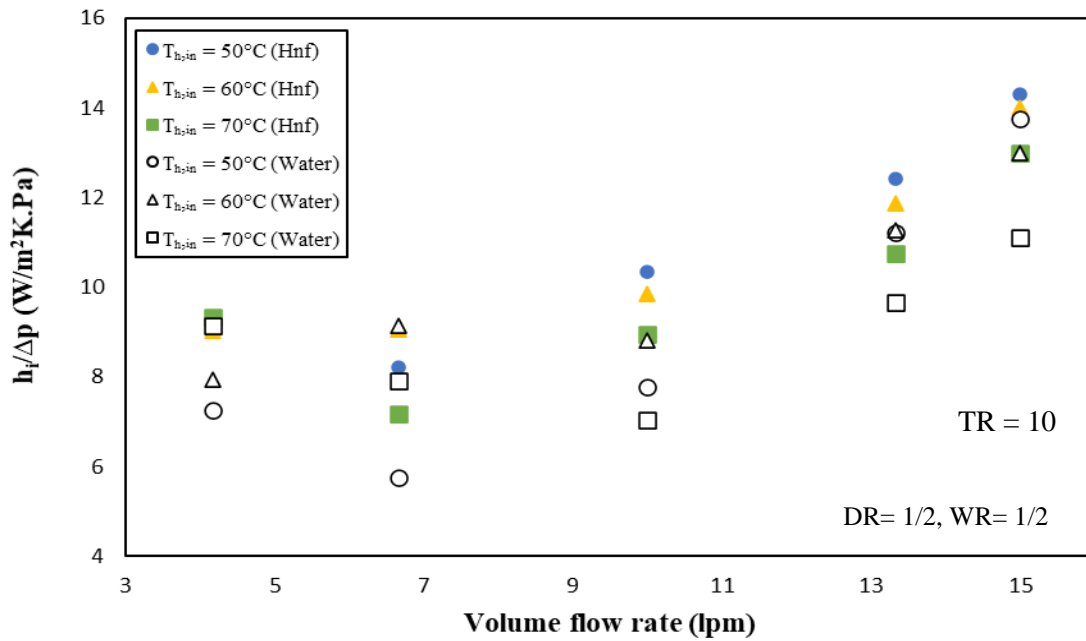


Figure 4.36. Variation of $h_i/\Delta p$ with the volume flow rate for different inlet temperatures

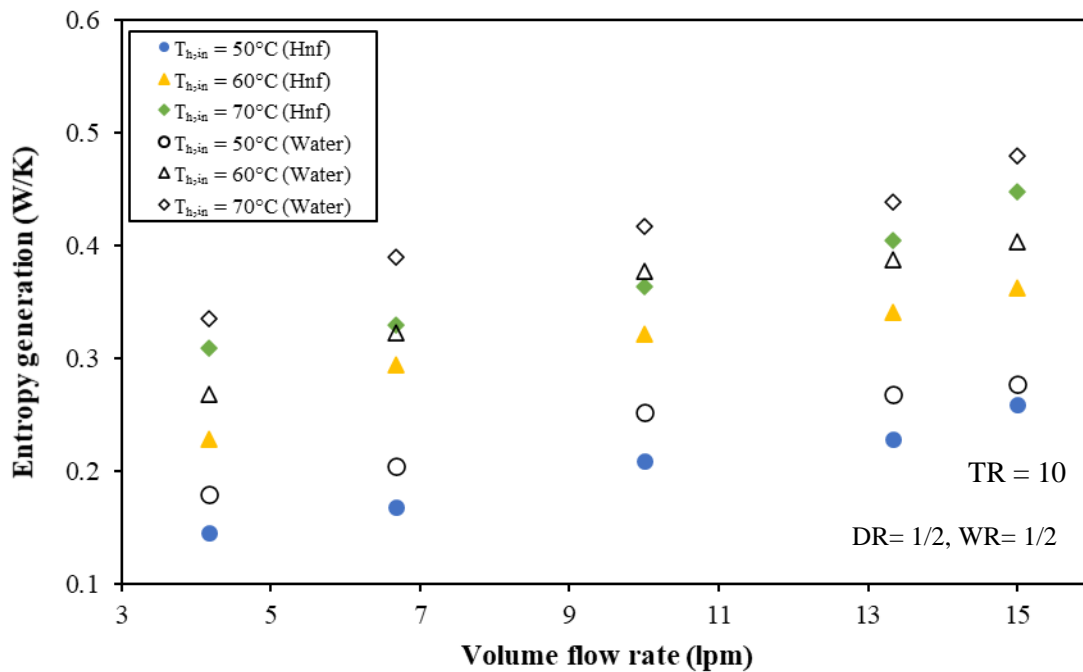


Figure 4.37. Variation of entropy generation with flow rate for different inlet temperatures

4.4.2 Experiment with Tapered wire coil inserts

4.4.2.1 Comparison of various hybrid nanofluids

Figs. 4.38 and 4.39 depict the heat transfer coefficient and pressure drop variation with nanofluid volume flow rate for different mono and hybrid nanofluid for the same wire coil configurations (plane wire coil) at the same volume concentration (0.01%). The outcomes indicate that while increasing the volume flow rate, both heat transfer coefficient and pressure drop increase. Wire coil insertions provide better heat transfer characteristics by diminishing the boundary layer thickness and thus increasing the turbulent flow intensity at a different radial distance in the tube. Since the thermal conductivity of nanoparticles is greater than that of the base fluid, which leads to promoting better heat transfer, the heat transfer coefficient of mono and hybrid nanofluid is greater than that of the base fluid (DI water). Fig.4.39 exhibits that the pressure drop of mono and hybrid nanofluid is greater than that of DI water. It is due to the fact that fluid viscosity increases by adding the nanoparticles in the base fluid, which leads to the enhancement of the pressure drop. Al_2O_3 +CNT hybrid nanofluid has maximum heat transfer coefficient and pressure drop compared to all other working fluids, as the thermal conductivity and viscosity are comparatively higher than that of other working fluids. The average enhancement of the heat transfer coefficient for Al_2O_3 +CNT hybrid nanofluid flowing in the inner tube with plane wire coil inserts is around 31%, while the pressure drop enhances 29.84% than that for DI water (base fluid).

The variation of Nusselt number and friction factor with Reynolds number for different mono and hybrid nanofluid for the same wire coil configurations (plane wire coil) at the same volume concentration (0.01%) are shown in Figs. 4.40 and 4.41. The results indicate that while increasing Reynolds number, Nu increases and friction factor decreases. The Nusselt number and friction factor increase due to the combined effects of enhancements in thermo-physical properties such as viscosity, heat capacity and thermal conductivity. Also,

the results indicate that the friction factor of all working fluids is higher than that of the DI water due to an increase in fluid viscosity. Al_2O_3 +CNT hybrid nanofluid shows a higher Nusselt number and friction factor among all working fluids. For the same high Reynolds number, $\text{Re} = 40,000$, the Nusselt number of Al_2O_3 +CNT hybrid nanofluid is enhanced by 14.34 % than that of the base fluid, 11.82% than that of PCM, 11% than that of Al_2O_3 , 10.05% than that of Al_2O_3 +PCM and 4.41% than that of CNT nanofluids, while for the same low Reynolds number, $\text{Re} = 8000$, the friction factor of Al_2O_3 +CNT hybrid nanofluid is enhanced by 17.09 % than that of the base fluid, 9.21% than that of Al_2O_3 +PCM, 7.31% than that of Al_2O_3 , 5.03% than that of CNT and 3.81% than that of PCM nanofluids respectively. At a high Reynolds number, say $\text{Re} = 40,000$, the friction factor of Al_2O_3 +CNT hybrid nanofluid shows a higher value while the value of friction factor for all other working fluids is nearly the same.

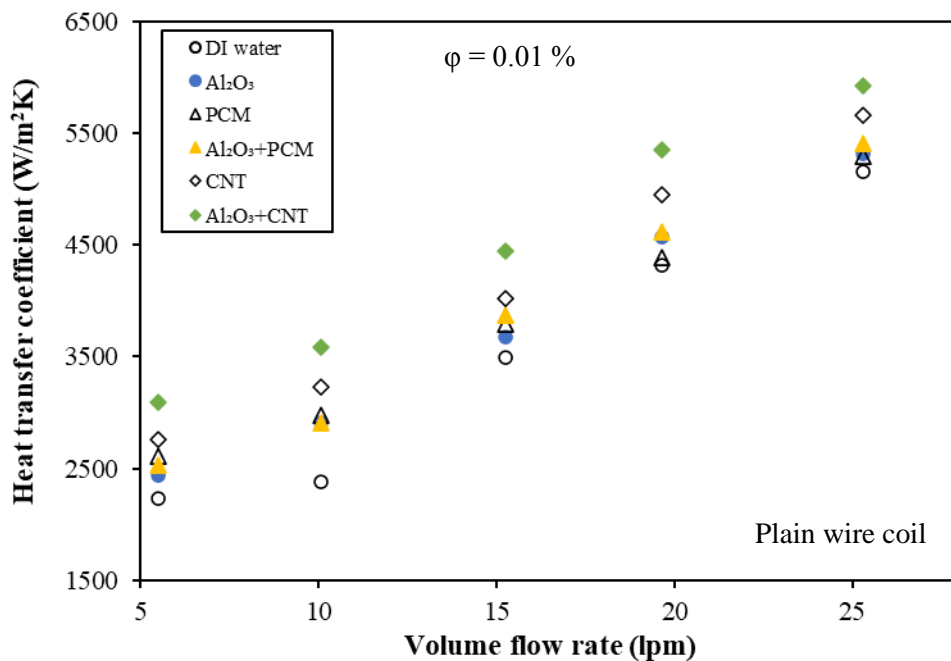


Figure 4.38. Variation of heat transfer coefficient with nanofluid flow rate for different mono and hybrid nanofluid

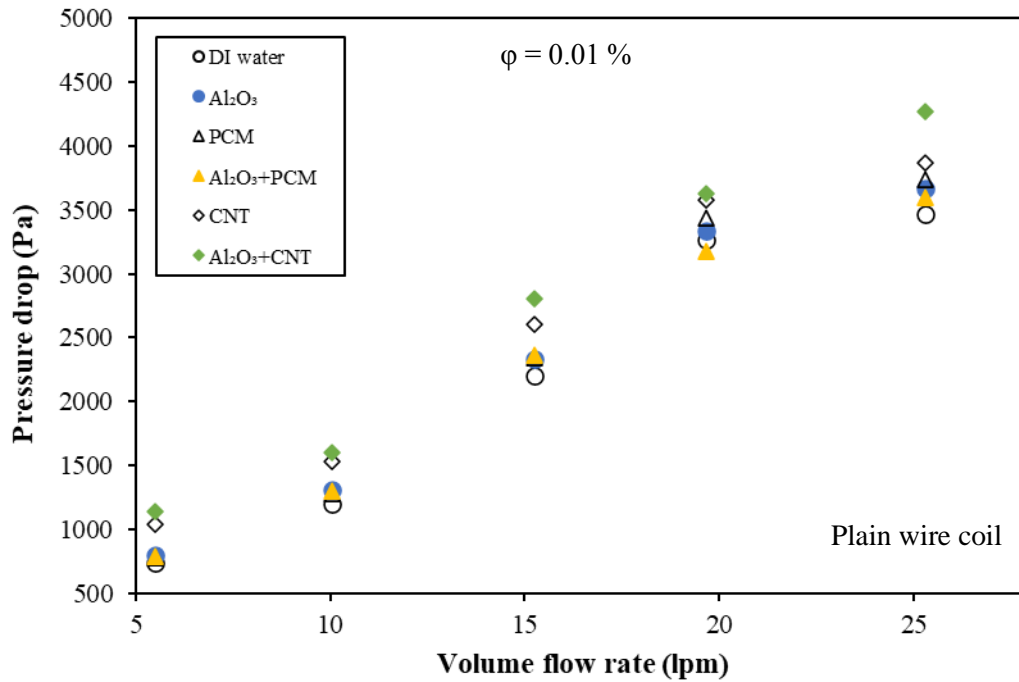


Figure 4.39. Variation of pressure drop with flow rate for different mono/hybrid nanofluid

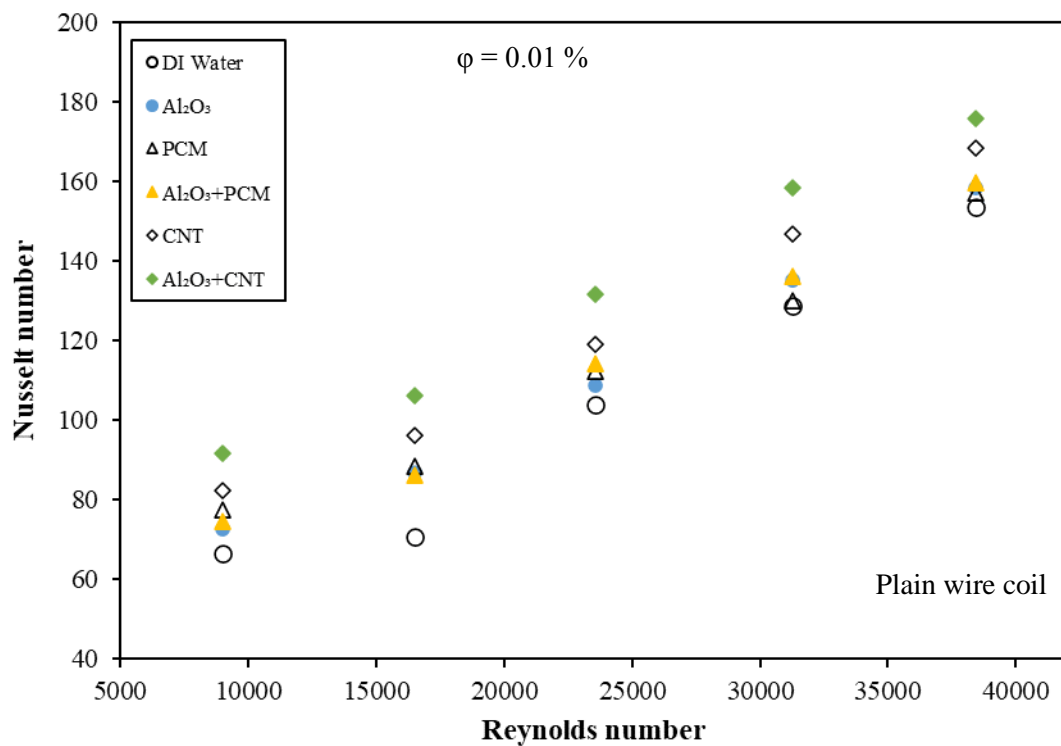


Figure 4.40. Variation of Nusselt number with Reynolds number for different nanofluids

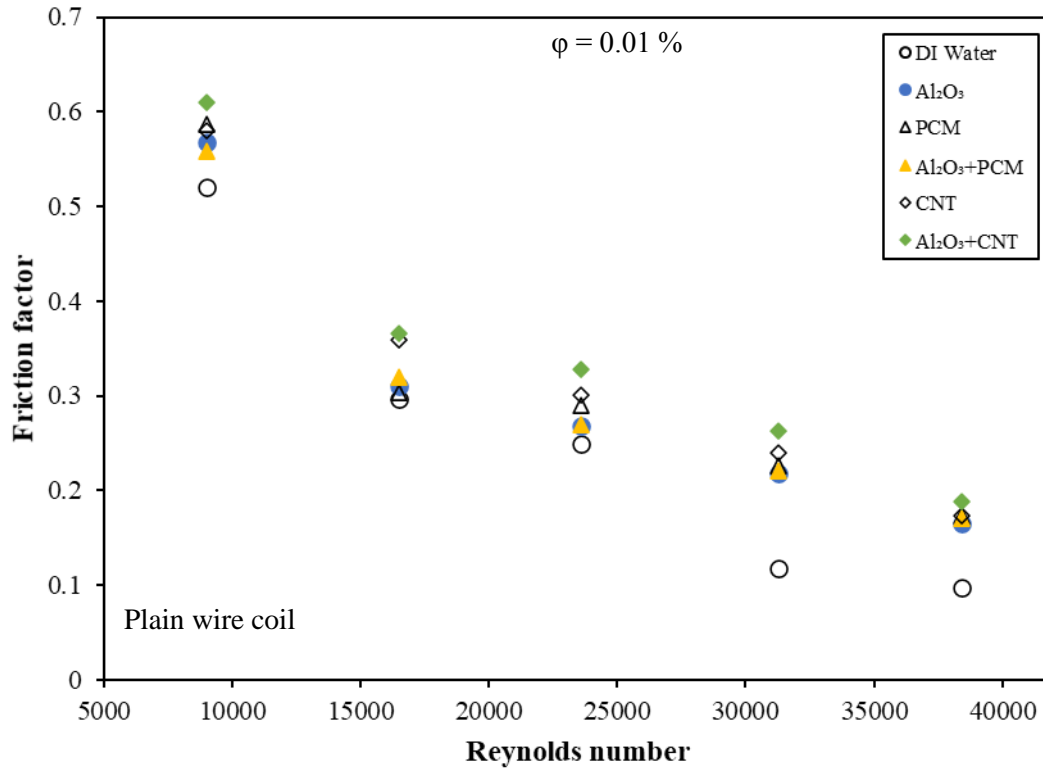


Figure 4.41. Variation of friction factor with Reynolds number for different nanofluids

The variation of $h/\Delta p$ ratio and entropy generation of hybrid nanofluid with the same wire coil configurations (plane wire coil) against the volume flow rate at the same volume concentration (0.01%) are depicted in Figs. 4.42 and 4.43. As seen in Fig 4.42, it is clear that with the increase in volume flow rate, the ratio $h/\Delta p$ decreases and diminishes up to the volume flow rate of 20 lpm and then increases for all cases of working fluids. In fact, while increasing the volume flow rate, the pressure drop increases much more than the heat transfer rate and this leads to a reducing $h/\Delta p$ ratio. The ratio $h_i/\Delta p$ yields maximum value at a low flow rate as h_i dominances over Δp at a low flow rate. Among all working fluids, Al_2O_3+CNT shows maximum $h_i/\Delta p$ value (3.37) at a low flow rate of 5 lpm. The $h/\Delta p$ ratio varies from 1.50 to 3.37 for Al_2O_3+CNT , 1.48 to 3.21 for CNT, 1.46 to 3.04 for Al_2O_3+PCM , 1.41 to 3.14 for PCM and 1.45 to 2.72 for Al_2O_3 nanofluid, respectively. In Fig 4.43, the total entropy generation increases with an increase in the hybrid nanofluid flow rate. With the

addition of solid nanoparticles in the base fluid, effective temperature difference decreases and pressure drop increases, and as a result, entropy generation due to heat transfer decreases and entropy generation due to pressure drop increases. Since the entropy generation, due to pressure drop, is found very less as compared to that due to heat transfer, the total entropy generation of mono and hybrid nanofluids is lower than that of the base fluid. The result shows that Al_2O_3 +PCM hybrid nanofluid shows a lower value of the total entropy generation among all working fluids. Compared to water, the average reduction in total entropy generation of Al_2O_3 +PCM hybrid nanofluid is found as 12.95% at the volume flow rate ranging from 5 to 25 lpm.

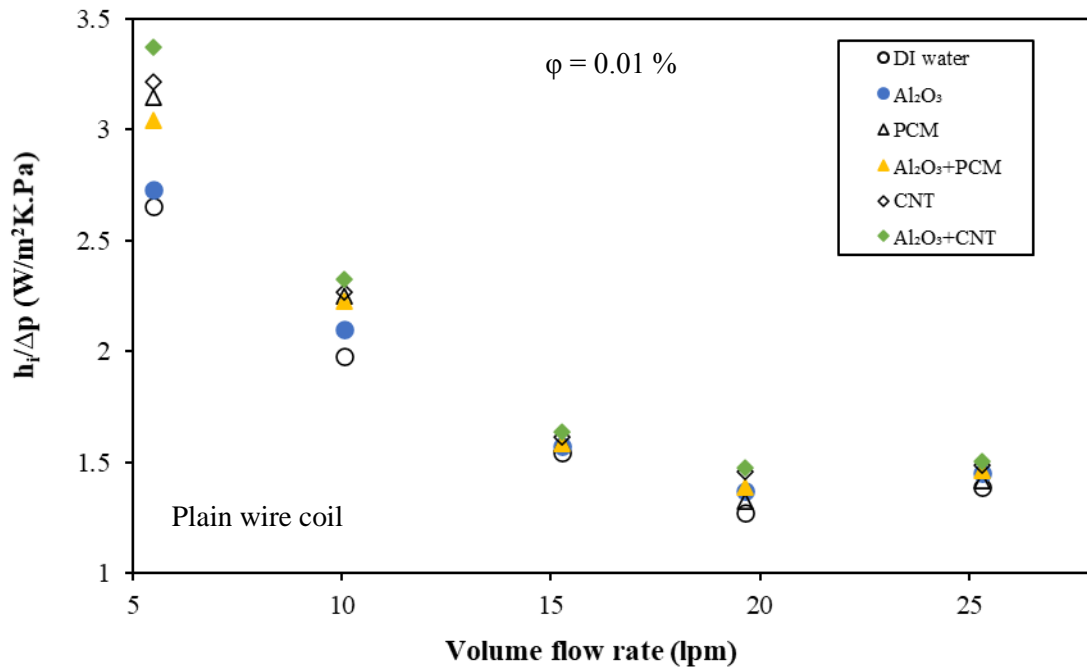


Figure 4.42. Variation of $h_i/\Delta p$ with nanofluid flow rate for different mono and hybrid nanofluid

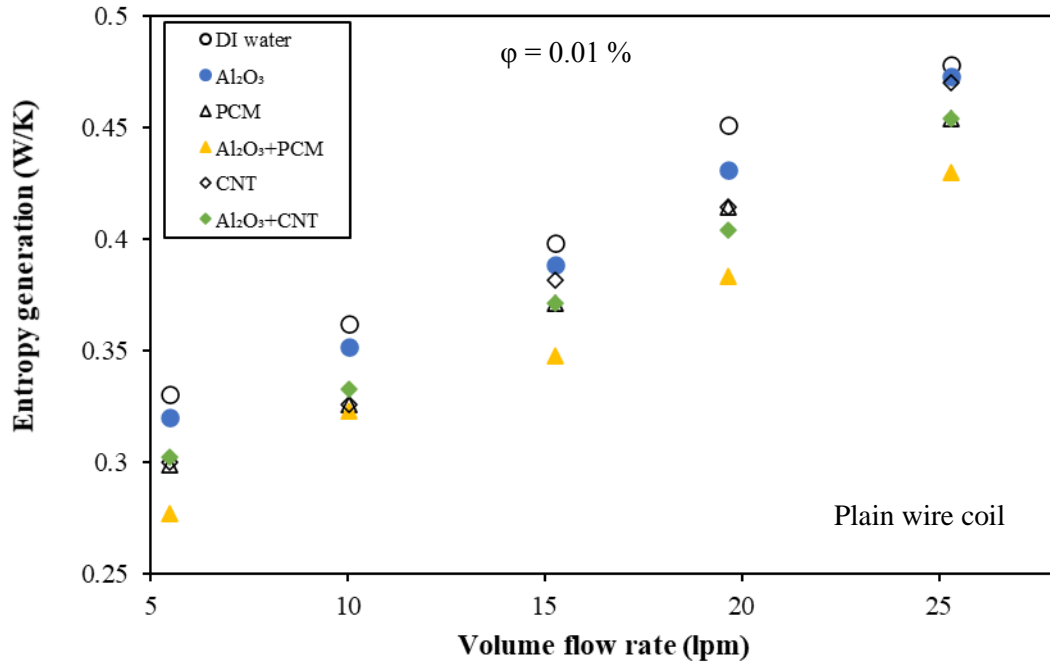


Figure 4.43. Variation of entropy generation with nanofluid flow rate for different nanofluids

4.4.2.2 Effect of volume concentration

The effect of volume concentration of mono and hybrid nanofluid on the heat transfer coefficient (h_i) and pressure drop (Δp) with plain wire coil inserts at a constant volume flow rate (15 lpm) are shown in Fig 4.44 and 4.45. The results show that h_i and Δp significantly increases with an increase in volume concentration. Al₂O₃+PCM hybrid nanofluid shows the maximum value of heat transfer coefficient, i.e., 4012.12 W/m²K followed by Al₂O₃ (3961.23 W/m²K) and PCM (3876.93W/m²K) while Al₂O₃+PCM hybrid nanofluid shows the higher value of pressure drop, i.e., 2636.14 Pa followed by PCM (2562.82 Pa) and Al₂O₃ (2536.14 Pa) respectively. When the volume concentration increases from 0.01 to 0.1%, the maximum augmentation of 7.87% in the heat transfer coefficient for Al₂O₃ and 11.63% in pressure drop for Al₂O₃+PCM was found respectively at the same flow rate of 15 lpm. The variation of Nusselt number and friction factor with different mono and hybrid nanofluid (Al₂O₃, PCM and Al₂O₃+PCM) for different volume concentrations (0.01%

and 0.1%) using plane wire coil inserts at the same volume flow rate of 15 lpm are illustrated in Figs. 4.46 and 4.47. The results found that with an increase in volume concentration from 0.01% to 0.1%, the Nusselt number and friction factor also increases. When the volume concentration increases from 0.01 to 0.1%, the average enhancement of Nu is 7.52 % for Al₂O₃, 3.64 % for Al₂O₃+PCM and 2.44 % for PCM, while the average enhancement of friction factor is 8.12% for Al₂O₃, 5.87 % for PCM, and 4.02% for Al₂O₃+PCM hybrid nanofluid respectively, for the same nanofluid volume flow rate.

Among all working fluids, Al₂O₃+PCM of volume concentration of 0.01% shows maximum $h_i/\Delta p$ value at a constant flow rate of 15 lpm using plane wire coil inserts, as shown in Fig 4.48. It is also observed that PCM and Al₂O₃+PCM of 0.01 vol.% concentration nanofluids have higher $h_i/\Delta p$ value than that of PCM and Al₂O₃+PCM of 0.1 vol.% concentration, respectively. It is due to the fact that at the higher volume concentration, the pressure drop increment dominants over the heat transfer coefficient at the same flow rate of 15 lpm. In Fig 4.49, the total entropy generation reduces with an increase in volume concentration from 0.01-0.1%. With the addition of nanoparticles in the base fluid, it leads to a decrease in the effective temperature differences and increases the pressure drop, which in turn decreases the total entropy generation. When the volume concentration increases from 0.01 to 0.1%, the maximum reduction of 10.73 % in total entropy generation is found for Al₂O₃ at the same flow rate of 15 lpm.

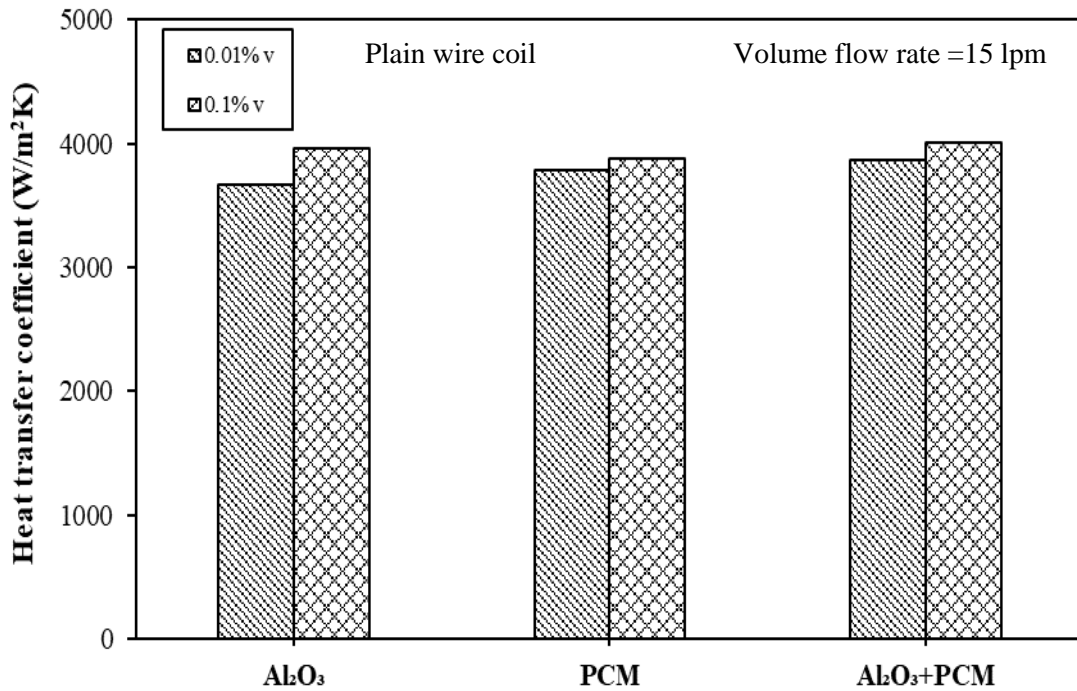


Figure 4.44. Variation of heat transfer coefficient with different mono and hybrid nanofluid for different volume concentration

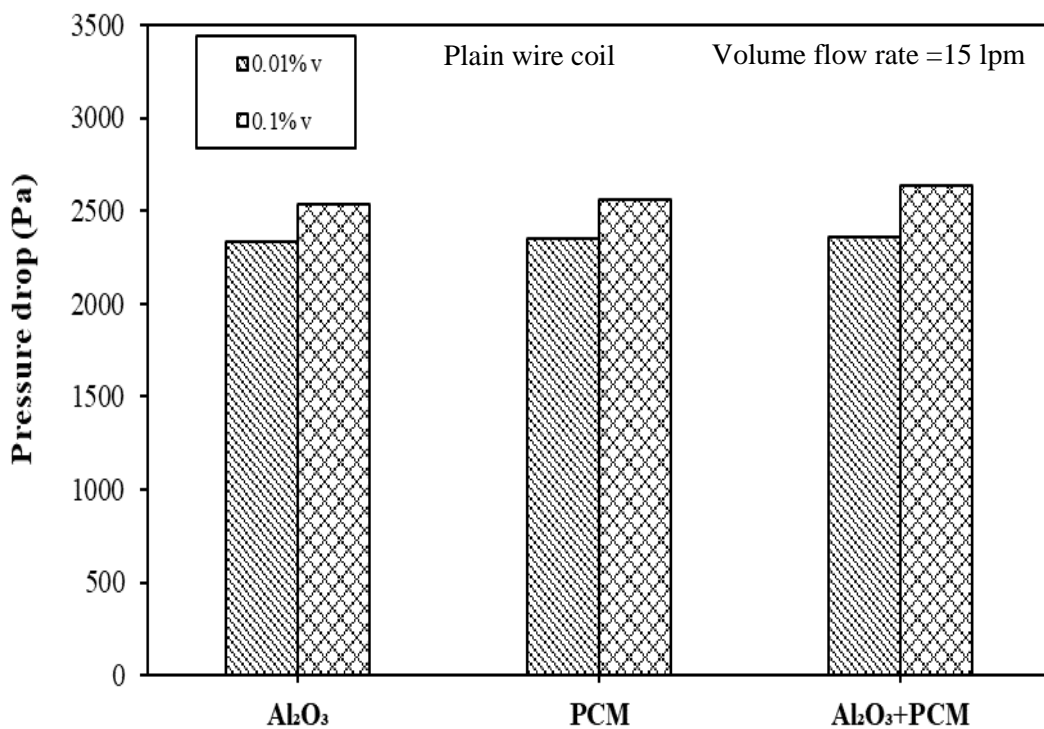


Figure 4.45. Variation of pressure drop with different mono and hybrid nanofluid for different volume concentration

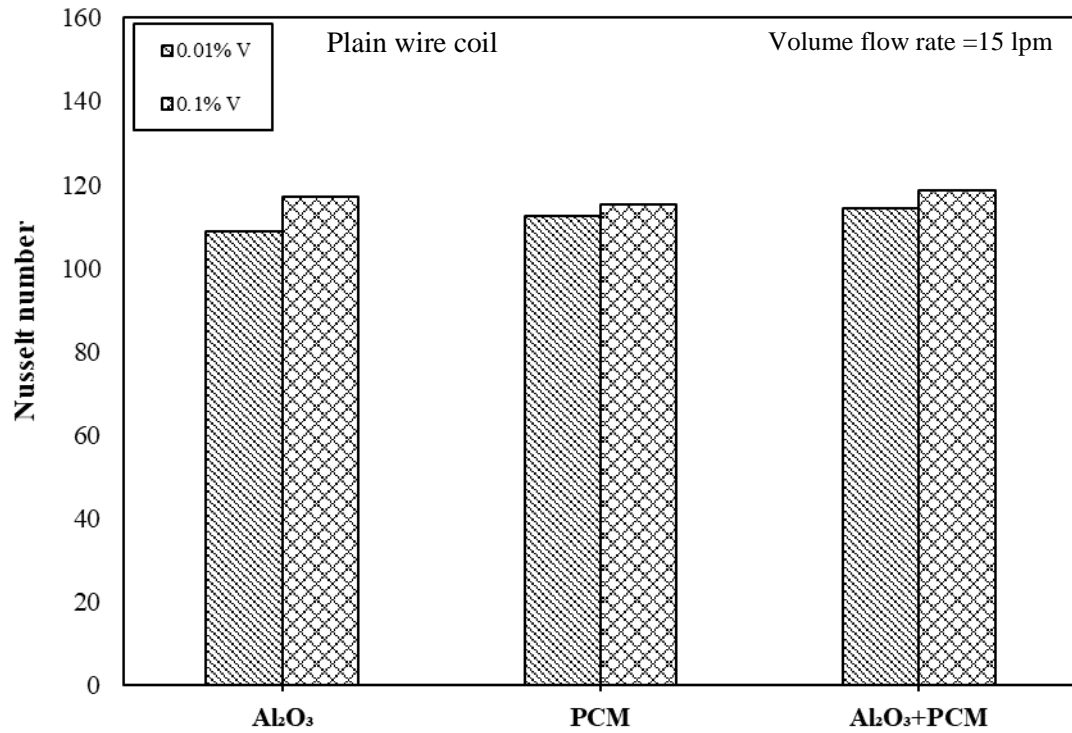


Figure 4.46. Variation of Nusselt number with different nanofluids and volume concentrations

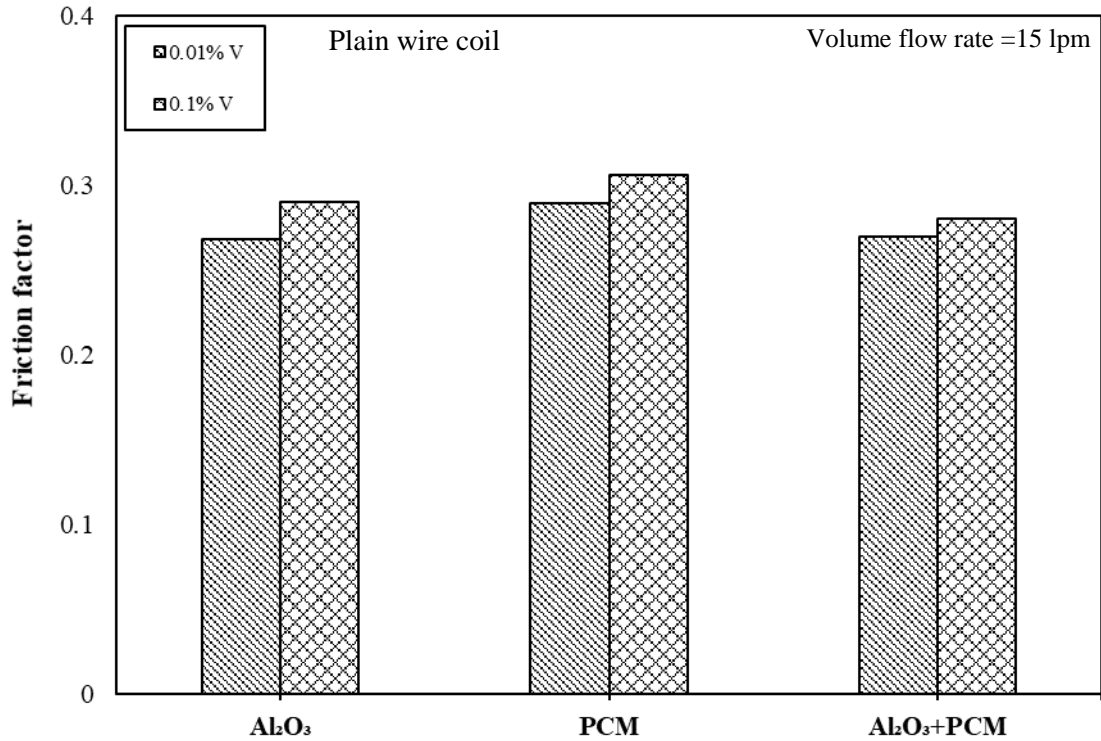


Figure 4.47. Variation of friction factor with different mono and hybrid nanofluid for different volume concentration

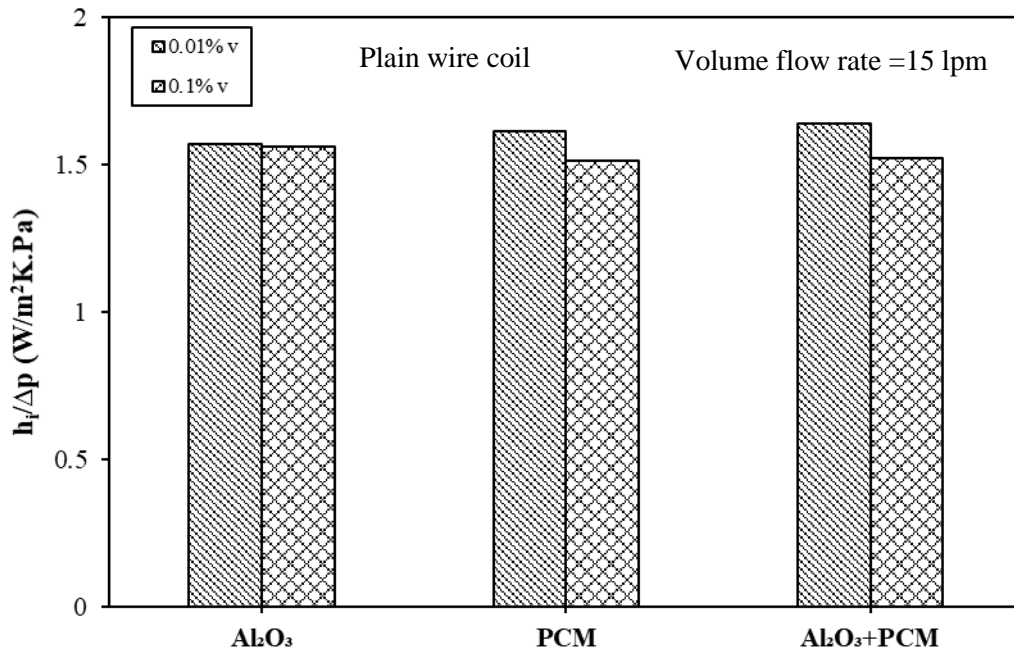


Figure 4.48. Variation of $h_i/\Delta p$ with different nanofluids and volume concentrations

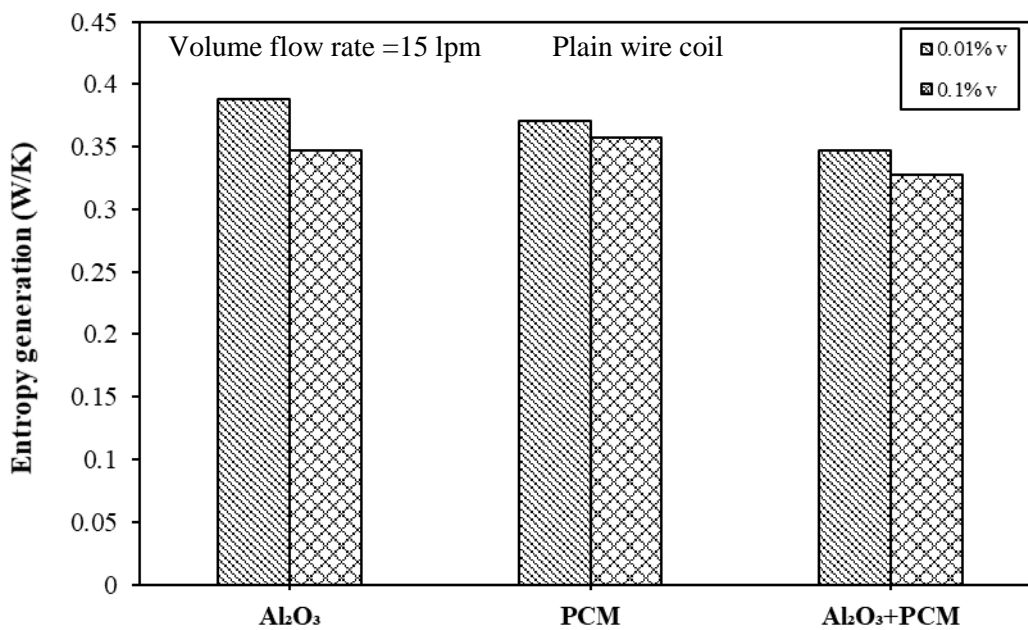


Figure 4.49. Variation of entropy generation with different nanofluid and volume concentration

4.4.2.3 Effect of different configurations

The heat transfer coefficient and pressure drop variation with different mono and hybrid nanofluid for different coil configurations (Plain tube, C-type, D-type and C-D type)

at the same volume concentration (0.01%) and volume flow rate of 15 lpm are depicted in Figs. 4.50 and 4.51. Tapered wire coil insertions provide better heat transfer characteristics by diminishing the boundary layer thickness and thus increasing the turbulent flow intensity at a different radial distance in the tube. The application of tapered wire coil inserts induces the separated flow along with the secondary flow along with the wire coil. The synergy of secondary flow and separated main flow brings out significant heat transfer enhancement. Also, the results expose that D-type wire coil exhibits enhanced heat transfer than that of other coil configurations because it provides higher contact surface area between fluid and wall surface when the fluid decelerates from D-type wire coil. Fig. 4.51 exhibits that the pressure drop increased by using tapered wire coil as compared to that of the plain tube. It is due to the fact that the fluid contact with the surface area of the wire coil is higher due to longer path flow, which leads to higher friction loss. D-type wire coil shows a high friction factor than that of the other coil configurations due to the disturbing of the flow at the entry of D-type wire coil turbulator and leads to a higher pressure drop across the length of the tube. The results reveal that Al_2O_3 +CNT hybrid nanofluid shows a higher heat transfer coefficient and pressure drop among all working fluids for different configurations. Using a D-type wire coil, the heat transfer coefficient of the Al_2O_3 +CNT hybrid nanofluid enhances around 55.26 % greater than that for the plane tube and 10.29 % more than that for C-type and 4.97 % more than that for C-D type wire coil, respectively. On the other hand, the friction factor of the Al_2O_3 +CNT hybrid nanofluid enhances around 86.66 % higher than that for the plane tube and 21.73 % greater than that for C-type and 4.47 % greater than that for C-D type wire coil, respectively using D-type wire coil. The comparisons of Nusselt number and friction factor of different mono and hybrid nanofluids for different coil configurations at a volume flow rate of 15 lpm are illustrated in Figs. 4.52 and 4.53. The results reveal that Al_2O_3 +CNT hybrid nanofluid shows a higher Nusselt number and friction factor among all

the working fluids. For the same $\text{Al}_2\text{O}_3+\text{CNT}$ hybrid nanofluid, using D-type wire coil, the Nusselt number enhances around 33.52 % greater than that for plain wire coil, 10.42 % more than that for C- type and 5.32 % more than that for C-D type respectively. On the other hand, using a D-type wire coil, the friction factor for the same $\text{Al}_2\text{O}_3+\text{CNT}$ hybrid nanofluid enhances around 27.06 % greater than that for plain wire coil, 21.48 % more than that for C- type and 6.20 % more than that for C-D type, respectively.

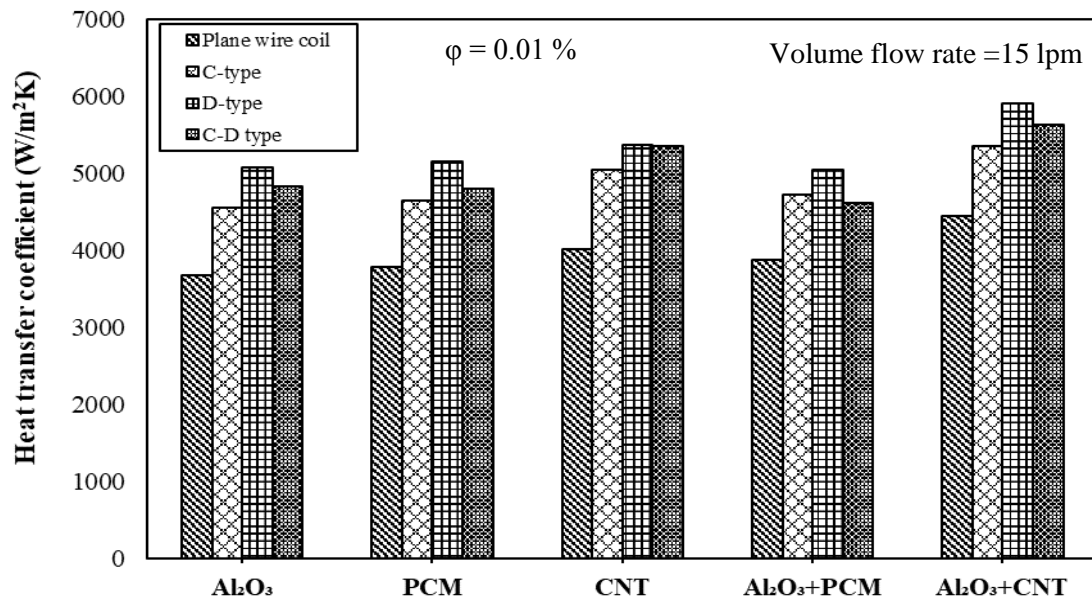


Figure 4.50. Variation of heat transfer coefficient with different mono and hybrid nanofluid for different coil configurations

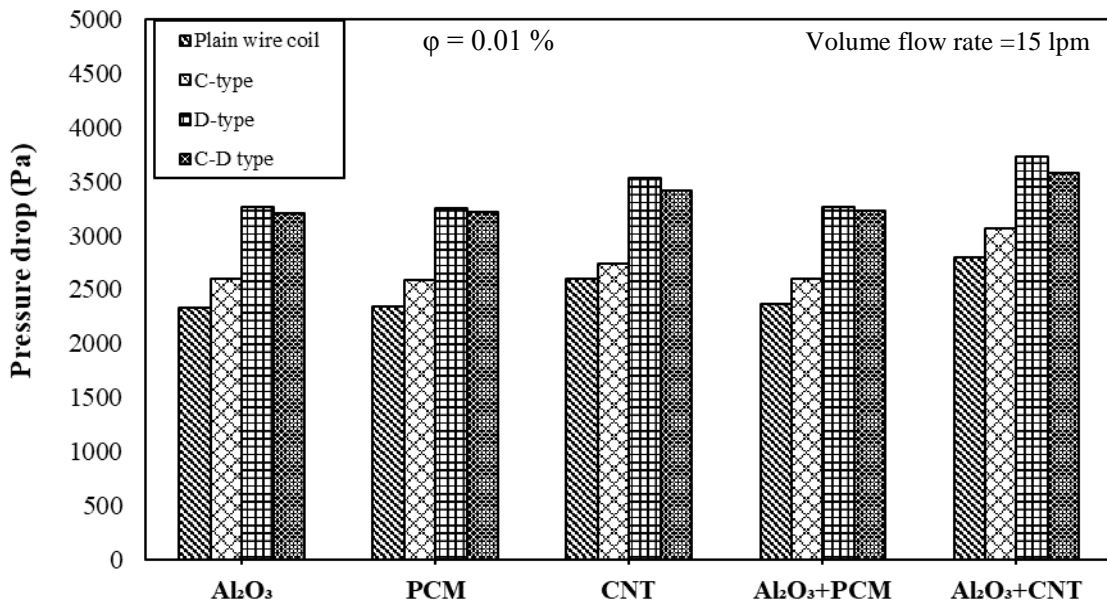


Figure 4.51. Variation of pressure drop with different mono and hybrid nanofluid for different coil configurations

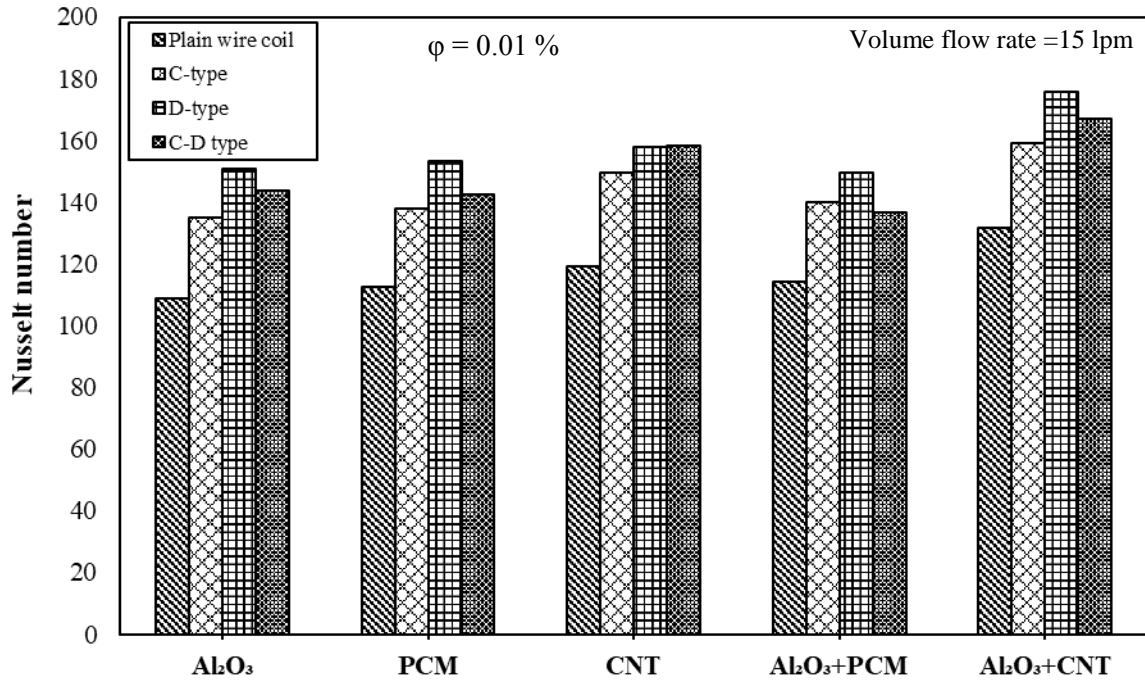


Figure 4.52. Variation of Nusselt number with different nanofluids and coil configurations

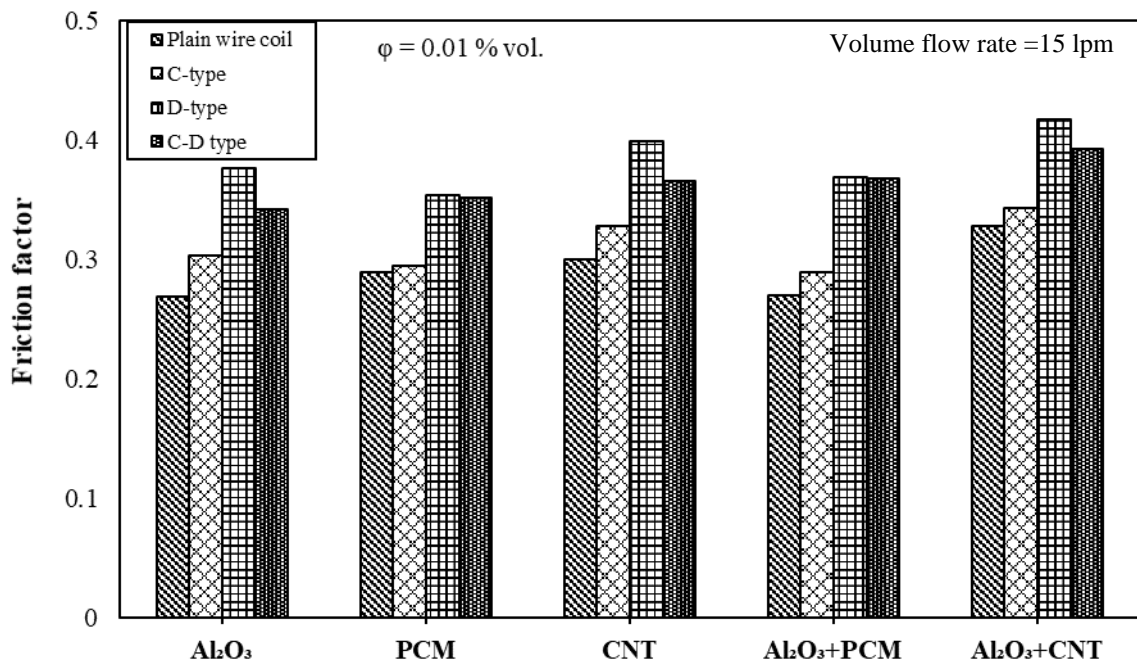


Figure 4.53. Variation of friction factor with different nanofluids and coil configurations

Figs. 4.54 and 4.55 show the effect of different mono and hybrid nanofluids on the $h/\Delta p$ ratio and entropy generation with different coil configurations at the same volume

concentration (0.01%) and volume flow rate of 15 lpm. The results reveal that the $h/\Delta p$ ratio of CNT nanofluid exhibits a higher value among all working fluids using C-type wire coil inserts. This is due to the fact that by using CNT nanofluid, the heat transfer coefficient dominates over the pressure drop at the flow rate of 15 lpm. For Al_2O_3 +CNT hybrid nanofluid, using C-type wire coil, the $h/\Delta p$ ratio of the hybrid nanofluid enhances by around 6.46 % more than that for the plain wire coil, 10.37 % more than that for D-type and 10.89 % more than that for C-D type, respectively, at a same volume flow rate of 15 lpm. In Fig.55, the result shows that Al_2O_3 +PCM hybrid nanofluid shows a lower value of the total entropy generation among all working fluids using D-type wire coil inserts. It may be noted that due to the presence of two different nanoparticles dispersed in the base fluid, effective temperature difference decreases and pressure drop increases, and as a result, entropy generation due to heat transfer decreases. For Al_2O_3 +PCM hybrid nanofluid, using D-type wire coil, the entropy generation reduces by around 11.86 % less than that for the plain tube, 8.43% less than that for C-type and 6.06 % lower than that for C-D type, respectively, at the same volume flow rate of 15 lpm.

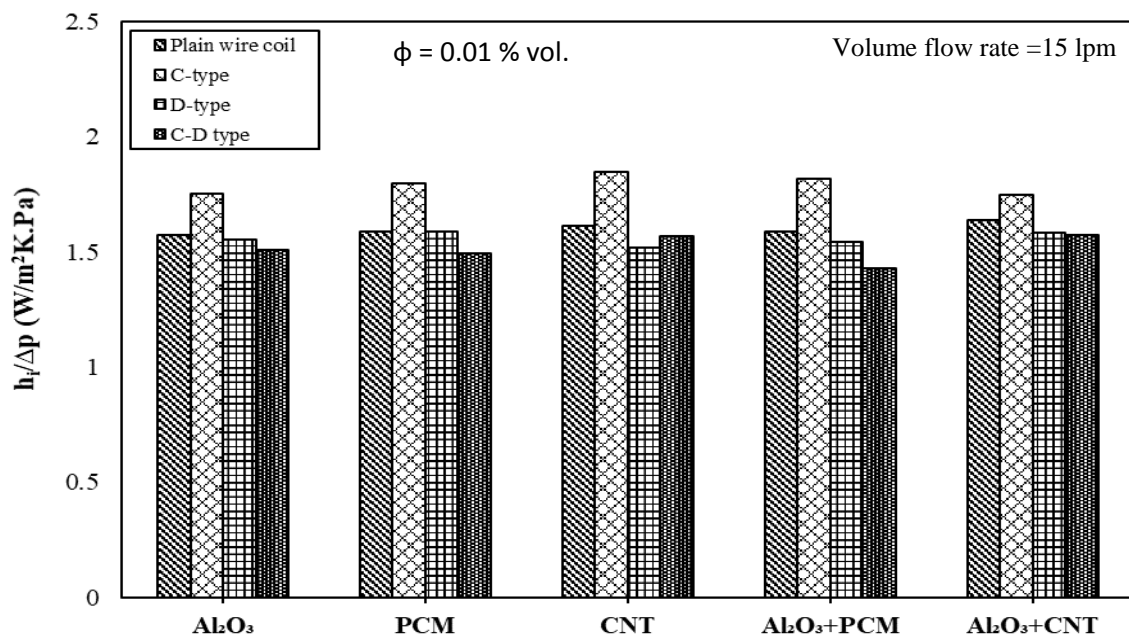


Figure 4.54. Variation of $h_i/\Delta p$ with different mono/hybrid nanofluids and coil configurations

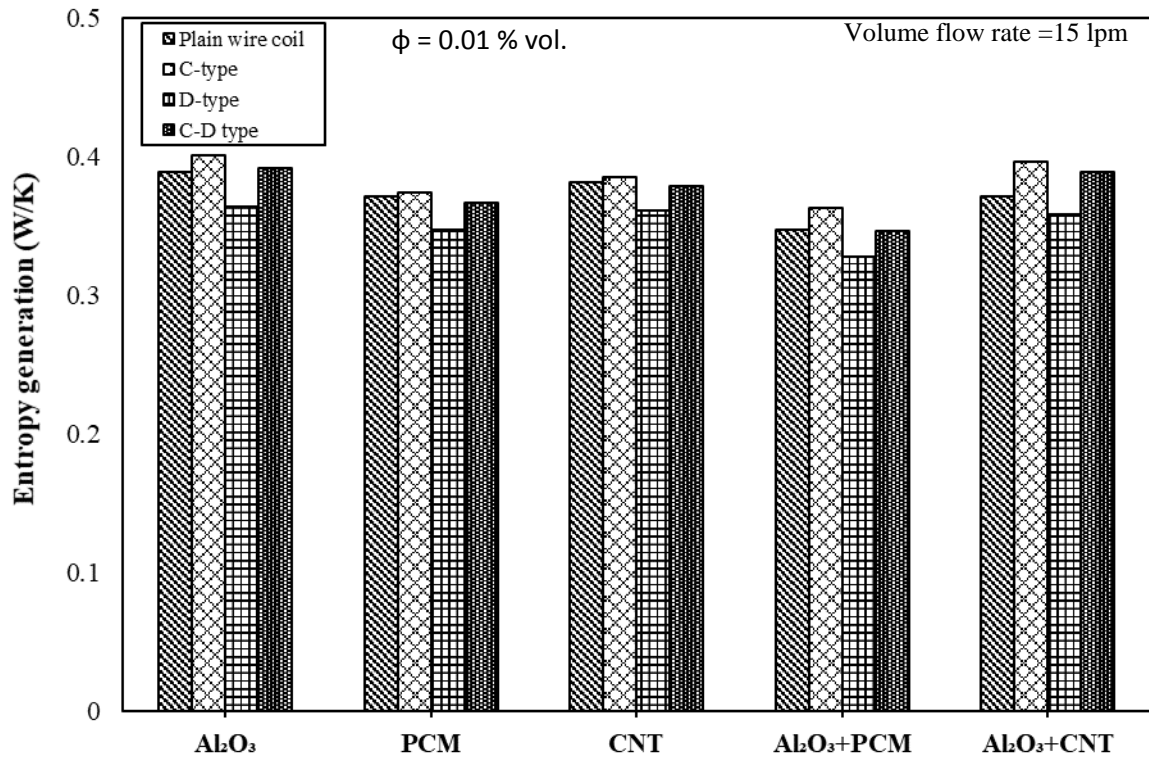


Figure 4.55. Variation of entropy generation with different nanofluids and coil configurations

4.4.2.4 Effect of hot nanofluid inlet temperature

Figs. 4.56 and 4.57 show the effect of hot nanofluid inlet temperature on heat transfer coefficient and pressure drop for different coil configurations at the same flow rate of 10 lpm. The results reveal that increasing the inlet temperature of the hot fluid increases the heat transfer coefficient and decreases the pressure drop. The heat transfer coefficient rises with an increase in temperature because of the augmentation in thermo-physical properties of the hybrid nanofluid, such as viscosity, density and thermal diffusivity. At the same instant, the pressure drop in the pipe also falls with the rise in inlet temperature as the fluid viscosity decreases with an increase in inlet temperature. At 70°C, using a D-type wire coil, the average heat transfer coefficient of the hybrid nanofluid enhances around 11.25 % greater than that of the hybrid nanofluid at 50°C and 2.20 % more than that of hybrid nanofluid at 60°C, respectively. In contrast, at 50°C, the pressure drop of the hybrid nanofluid enhances

around 9.09 % more than that of hybrid nanofluid at 70°C and 2.12 % more than that of hybrid nanofluid at 60°C, respectively. The variations of Nusselt number and friction factor of hybrid nanofluid for different configurations with different inlet temperatures of 50°C, 60°C and 70°C at a volume flow rate of 10 lpm are illustrated in Figs. 4.58 and 4.59. The results show that the Nusselt number increases and the friction factor decreases with increasing the inlet temperature of hybrid nanofluid. Using a D-type wire coil, the maximum value of the Nusselt number for water shows 304.7 at 70°C, followed by 288.7 at 60°C and 273.4 at 50°C, respectively. At 70°C, using a D-type wire coil, the average Nusselt number of the hybrid nanofluid enhances around 11.43 % greater than that of the water and 8.05 % more than that of hybrid nanofluid at 50°C, respectively. Using a D-type wire coil, the maximum value of friction factor for water shows 0.2426 at 50°C, followed by 0.2402 at 60°C and 0.2377 at 70°C, respectively. In contrast, at 50°C, the average friction factor of the hybrid nanofluid enhances around 13.96 % more than that of water and 8.1 % more than that of hybrid nanofluid at 70°C, respectively.

Figs. 4.60 and 4.61 show the effect of the inlet temperature of hybrid nanofluid on the $h/\Delta p$ ratio and entropy generation with different coil configurations at the volume flow rate of 10 lpm. The results reveal that with the rise in hybrid nanofluid inlet temperature, both the $h/\Delta p$ ratio and entropy generation increase. This is due to the fact that the increase in hybrid nanofluid inlet temperature leads to a reduction of fluid velocity as well as viscosity and thus, reduction of the pressure drop. For example, at an inlet temperature of 70°C, using a D-type wire coil, the $h/\Delta p$ ratio of the hybrid nanofluid enhances by around 20.25 % more than that of hybrid nanofluid at 50°C for the same volume flow rate of 10 lpm. The result indicates that with the increase in hybrid nanofluid inlet temperature, the total entropy generation increases for all types of wire coil configurations because of an increase in the overall temperature difference of the heat exchanger. It may be known that with an increase in temperature, the

fluid properties improve (thermal conductivity increases and viscosity decreases) and hence both heat transfer and friction factor-related entropy generations will decrease for some difference between hot and cold inlet temperatures. At 70°C, the reduction of 17.43% in total entropy generation has been found for D-type wire coil as compared to a smooth tube using hybrid nanofluid.

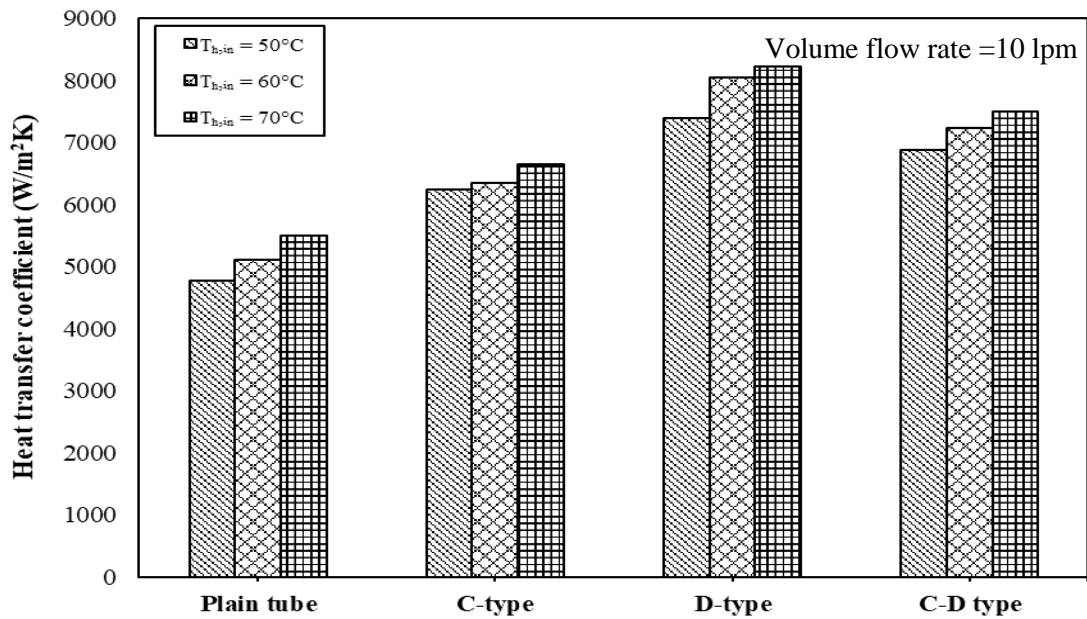


Figure 4.56. Variation of heat transfer coefficient with different configurations of tapered wire coil inserts for different inlet temperatures

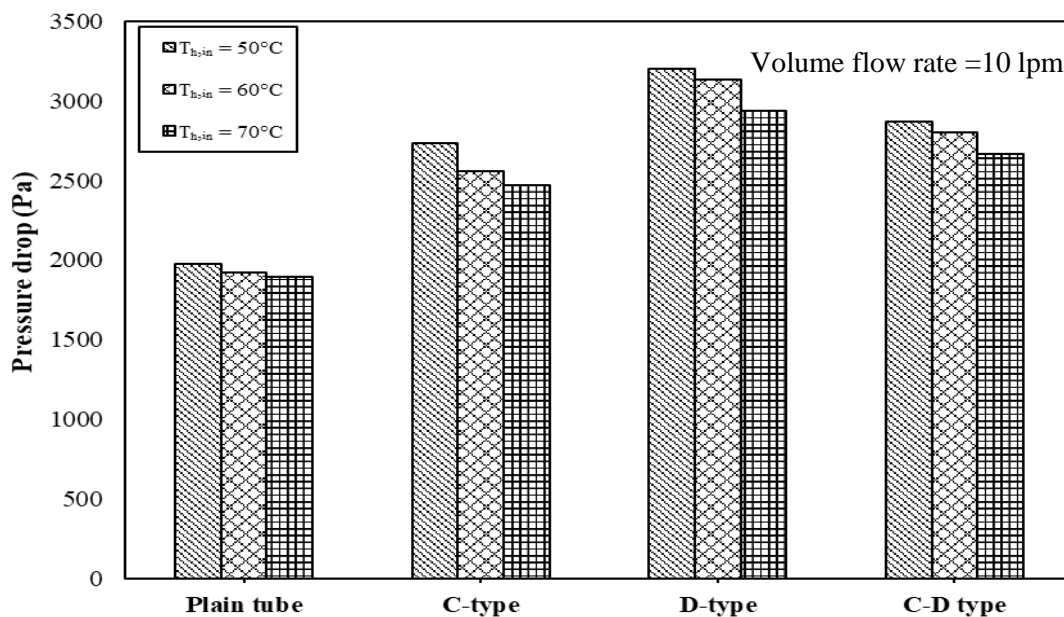


Figure 4.57. Variation of pressure drop with different configurations of tapered wire coil inserts for different inlet temperatures

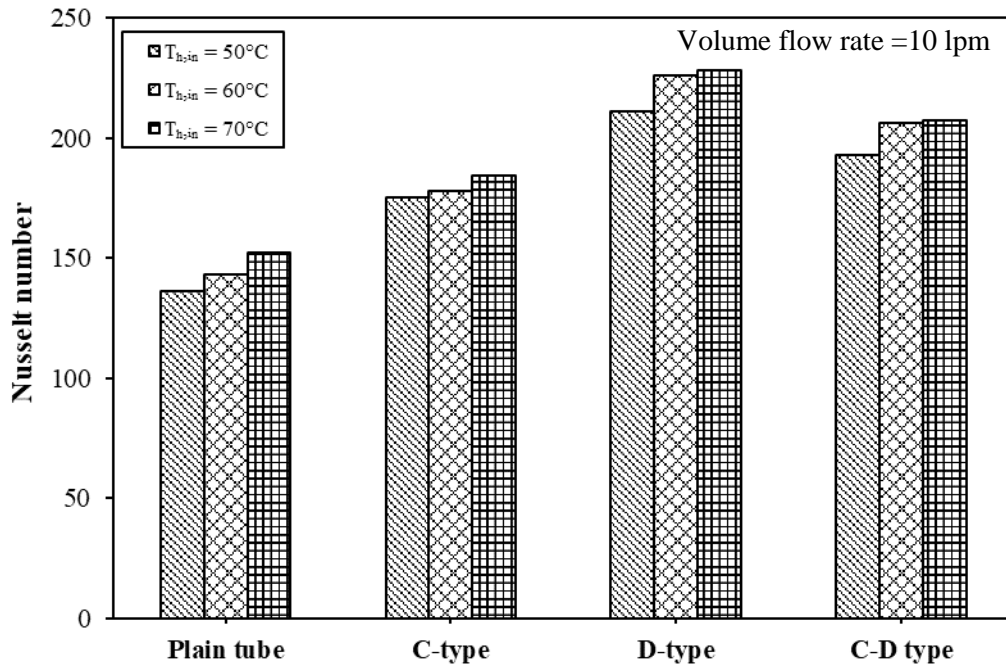


Figure 4.58. Variation of Nusselt number with different configurations of tapered wire coil inserts for different inlet temperatures

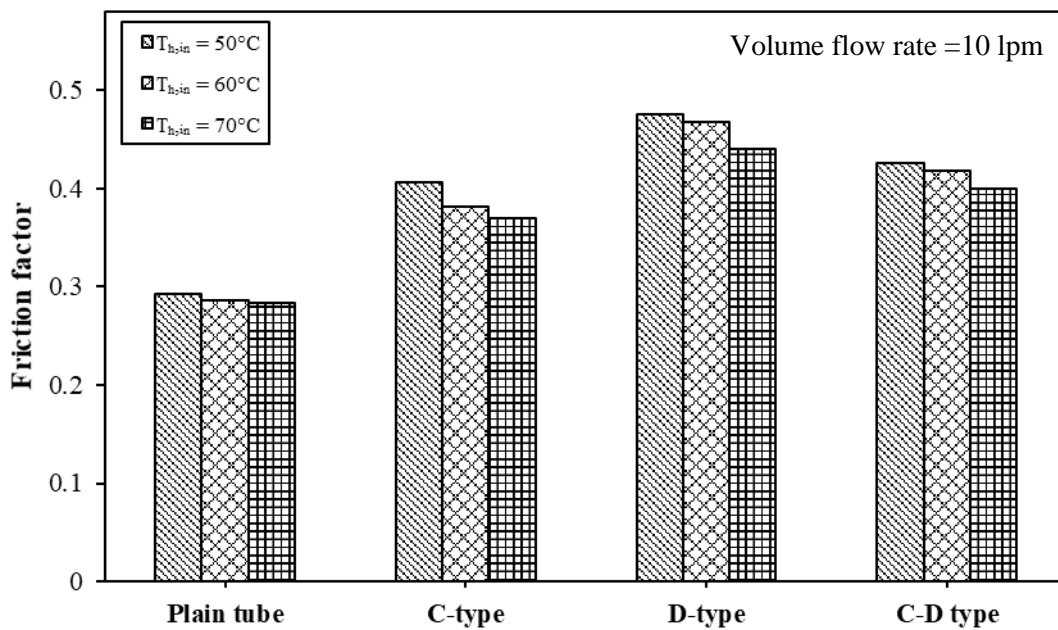


Figure 4.59. Variation of friction factor with different configurations of tapered wire coil inserts for different inlet temperatures

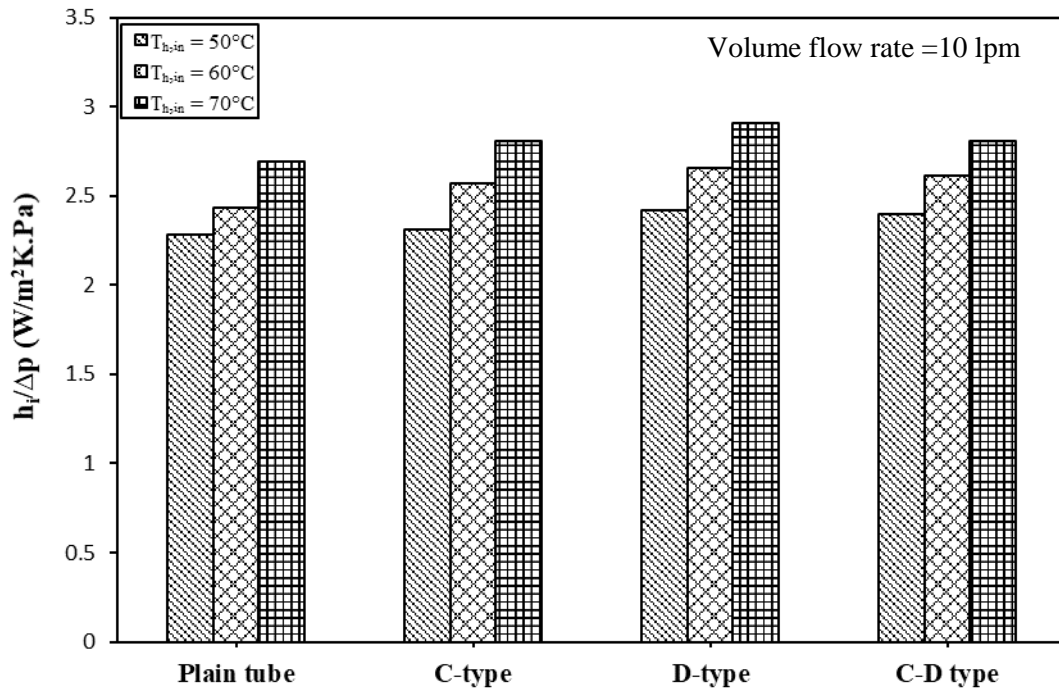


Fig. 4.60. Variation of $h_i/\Delta p$ with different configurations of tapered wire coil insert for different inlet temperatures

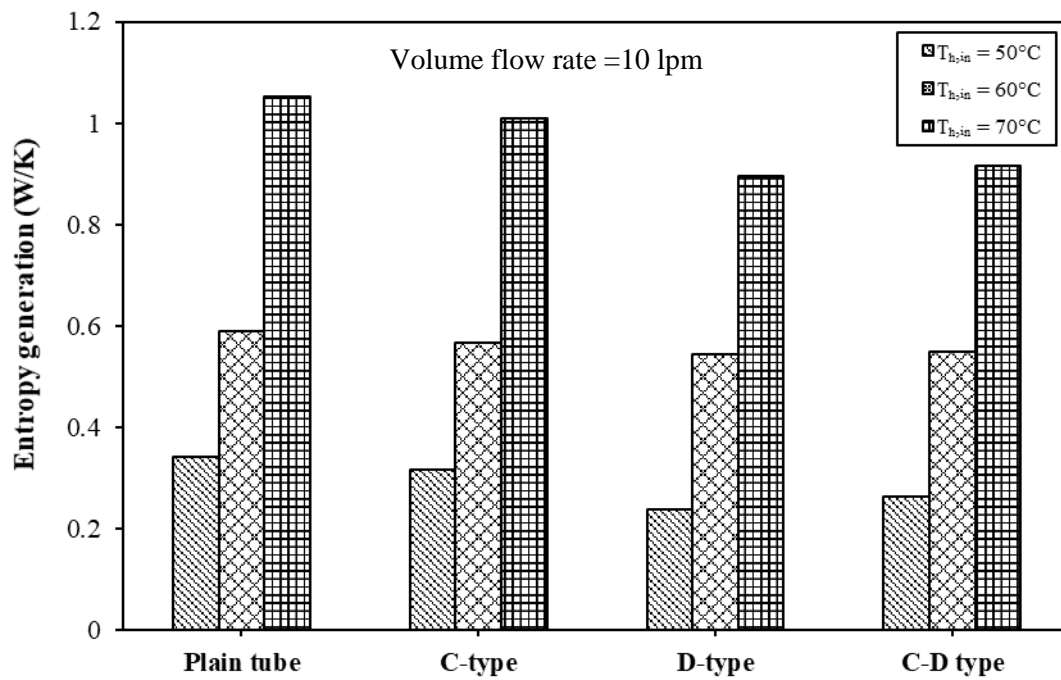


Fig. 4.61. Variation of entropy generation with different configurations of tapered wire coil inserts for different inlet temperatures

4.4.3 Comparison of effectiveness with/without enhancers

The effectiveness of the double pipe heat exchanger is the ratio of the temperature difference of the cold nanofluids (minimum fluid) to the maximum temperature difference between cold and hot fluids, which is given by;

$$\varepsilon = \frac{(T_{nf,out} - T_{nf,in})}{(T_{h,in} - T_{nf,in})} \quad (4.19)$$

Fig 4.62 shows the variation of the effectiveness with Reynolds number for different configurations of enhancers with the same 0.01 % Al_2O_3 +CNT hybrid nanofluid. It can be observed that the effectiveness decreases with an increase in Reynolds number. The effectiveness of the double pipe heat exchanger with enhancers and hybrid nanofluid is greater than that without enhancers and nanofluid. Also, the result reveals that tapered wire coils show a higher value of effectiveness than that of the V-cut twisted tapes at the same Reynolds number. This is due to the fact that the tapered wire coils provide a higher heat transfer coefficient than that of the V-cut twisted tapes, which leads to an increase in the temperature difference of the inner tube, which in turn increases the effectiveness. Among all enhancers, the D-type wire coil shows a higher value of effectiveness than other configurations of the enhancers. As compared to the plain tube with DI water, the effectiveness of the double pipe heat exchanger enhances around 39.41 % using D-type wire coil and hybrid nanofluid. The value of effectiveness of the double pipe heat exchanger ranges from 0.043 to 0.126. The effectiveness obtained is very low due to the smaller heat transfer area of the experimental double pipe heat exchanger compared with that of an industrial double pipe heat exchanger.

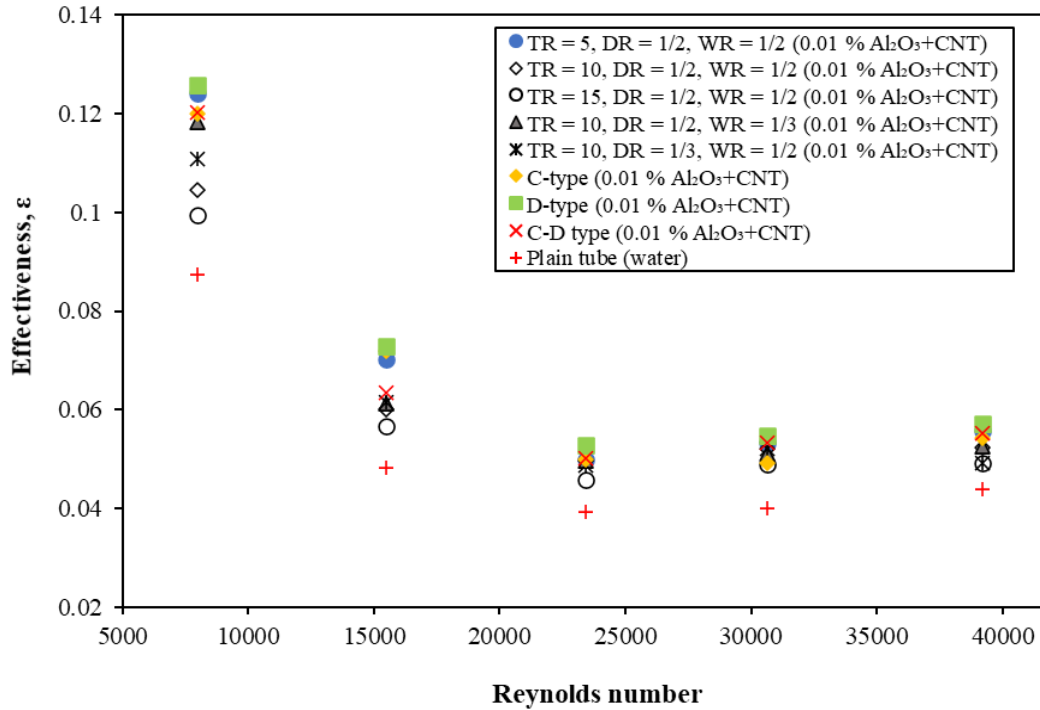


Fig. 4.62. Variation of effectiveness with Reynolds number for different configurations of enhancers and fluids

4.4.4 Comparison between the twisted tape and wire coil

The enhancements of the h , Nu , Δp , f , $h/\Delta p$ and S_{gen} at the mean condition (twisting ratio of 10, depth ratio of 1/2, width ratio of 1/2, D-type tapered wire coil, the mean flow rate of 15 lpm and nanofluid inlet temperature of 30°C) as compared to water in the plain tube are summarized in Table 4.7 and 4.8. As shown in the tables, the parameter enhancement is more predominant for using the enhancer (twisted tape and wire coil) as compared to using nanofluids. It implies that the change in flow structure by the use of the enhancer is much more significant as compared to property enhancement and slip mechanisms by using nanofluids. The maximum enhancement of h , Nu , Δp , f , $h/\Delta p$ and S_{gen} using V-cuts twisted tape with nanofluid are 67.24 %, 66.25%, 157.14%, 167.21%, 34.96 % and 23.62 % (reduction) respectively, at the mean condition as compared to water in the plain tube. On the other hand, using tapered wire coil with nanofluid, the maximum enhancement of h , Nu , Δp ,

f , $h/\Delta p$ and S_{gen} are 114.17%, 113.68 %,700%, 1288.50 %, 73.22% and 24.14 % (reduction) respectively, as compared to water in the plain tube.

Table 4.7. Maximum improvements of various parameters by using twisted tape and nanofluids at the mean operating condition.

Parameters	Plain tube with nanofluid	Plain twisted tape with nanofluid	V-cuts twisted tape with water	V-cuts twisted tape with nanofluid
h	16.16 %	62.51%	18.11%	67.24%
Nu	15.80 %	62.78%	18.09%	66.25 %
Δp	14.28%	128.57%	111.42%	157.14 %
f	12.56 %	139.41%	108.66%	167.21 %
$h/\Delta p$	7.15 %	28.90%	44.29%	34.96 %
S_{gen}	7.10 % (reduction)	10.85% (reduction)	14.92 (reduction)	23.62% (reduction)

Table 4.8. Maximum improvements of various parameters by using tapered wire coil & nanofluids at the mean operating condition.

Parameters	Plain tube with nanofluid	Plain wire coil with nanofluid	Tapered wire coil with water	Tapered wire coil with nanofluid
h	16.16 %	61.25%	74.84 %	114.17%
Nu	15.80 %	60.03 %	74.27 %	113.68 %
Δp	14.28%	500%	585.71 %	700%
f	12.56 %	992.80%	977.92 %	1288.50 %
$h/\Delta p$	7.15 %	72.24 %	68.84 %	73.22 %
S_{gen}	7.10 % (reduction)	19.49 % (reduction)	15.66 % (reduction)	24.14 % (reduction)

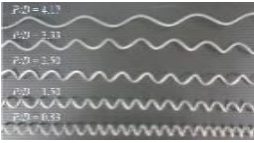
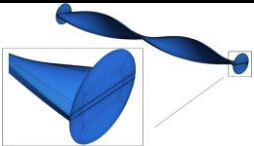
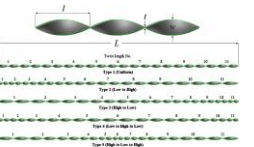
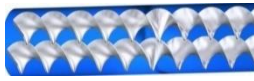
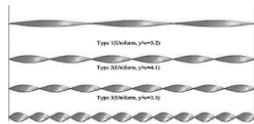

Table 4.9 shows the Nusselt number value obtained by the present combination (nanofluid and enhancers) is compared with the Nu values of different nanofluids with enhancers from the previous studies. The other nanofluids and enhancers subjected to comparison include TiO₂-SiO₂ nanofluid with wire coil of different pitch ratio by **Hamid et al. (2019)**, CMC-CuO nanofluid with the twisted tape of different twist ratio by **Bazdidi-Tehrani et al. (2019)**, Cu/W nanofluid with twisted tape with different twist length by **Khoshvaght-Aliabadi and Eskandari (2015)**, GnP-Pt/W nanofluid with twin co-twisted tape by **Bahiraee et al. (2018)**, Fe₃O₄/W nanofluid with twisted tape with different pitch length by **Aghayari et al. (2020)**, Graphite-SiO₂ nanofluids with the quad-channel twisted tape of different length by **Dalkilic et al. (2019)** and water-based Al₂O₃ nanofluids with plain wire coils of different pitches by **Akyurek et al. (2018)**. Based on the result, it can be concluded that at low volume concentration (0.01% and 0.1%) of studied mono/ hybrid nanofluid with enhancers (modified twisted tape and modified tapered wire coil) provide superior Nu value than other combination of nanofluid and enhancers from the previous studies.


4.5 Highlights

- Using enhancer (V-cuts twisted tapes and tapered wire coil), heat transfer coefficient and pressure drop considerably increase with an increase in the nanofluid flow rate. In addition, h_i and Δp are higher than that of the DI water and increase with an increase in volume concentration. Also, h_i and Δp increase with decreasing the twist ratio, increase in DR and decrease in WR in the case of all working fluids. D-type wire coil exhibits higher heat transfer and pressure drop than that of other coil configurations.

- The ratio $h_i/\Delta p$ decreases with an increase in nanofluid flow rate for all cases of working fluids using enhancer in most cases. Among all working fluids, Al_2O_3+CNT shows maximum $h_i/\Delta p$ value at a low flow rate of 5 lpm.

Table 4.9. Comparison of presently obtained Nu values with previous studies

Authors	Nanofluids	Enhancer	Conditions	Nu value range
Present Study	Al_2O_3 , PCM, CNT Al_2O_3+PCM , Al_2O_3+CNT (Vol % = 0.01 and 0.1)	V-cut TT and TWC	$8000 < Re < 40,000$	60-250
Hamid et al. (2019)	TiO_2-SiO_2 (Vol % = 0.5-3)	 Wire coil, P/D = 0.83-4.17	$2300 < Re < 12,000$	40-350
Bazdidi-Tehrani et al. (2019)	CMC-CuO (Vol % = 0.1-1.5)	 TT, TR = 5, 10, 15 and 83	$2500 < Re < 10,000$	250-1300
Khoshvaght-Aliabadi and Eskandari (2015)	Cu/W (Vol % = 0-0.3)	 TT, Width of tape = 14.5 mm, length of tape = 1100mm, Twist length = 50-150 mm	$7500 < Re < 15,000$	70-180
Bahiraee et al. (2018)	GnP-Pt/W (Vol % = 0.02-0.1)	 Twin Co-TT, TR = 2.5, 3 and 3.5	$5000 < Re < 20,000$	110-375
Aghayari et al. (2020)	Fe_3O_4/W (Vol % = 0.08 and 0.1)	 TT, TR = 2.5-5.2	$5000 < Re < 28,500$	30-220
Dalkilic et al. (2019)	Graphite- SiO_2 (Vol % = 0.5 and 0.1)	 Quad channel TT, TR = 5, Length of tape = 14-42 cm	$3400 < Re < 11,000$	30-95

Akyurek et al. (2018)	$\text{Al}_2\text{O}_3/\text{W}$ (Vol % = 0.4 and 1.6)		4000 Re <math>< 20,000</math>	90-470
		Plain wire coil Pitch= 25 and 39 mm		

- The entropy generation of all working fluids is lesser than that of the DI water. Among all working fluids, $\text{Al}_2\text{O}_3+\text{PCM}$ shows the lowest entropy generation using enhancer.
- For a given twist, depth and width ratios, Nu and f increase with decreasing the nanofluid inlet temperature. Nu enhancement of hybrid nanofluid at 50°C is 13.57 % more than that at 70°C; while friction factor increment of hybrid nanofluid is 8.74 % greater than that at 70°C. With the increase in inlet temperature from 50°C to 70°C, the Nusselt number of hybrid nanofluid enhances around 8.0% and the friction factor of hybrid nanofluid decreases by 8.1% using D-type wire coil inserts in a double tube heat exchanger.
- The parameter enhancement is more predominant for using enhancer (twisted tape and wire coil) with nanofluids, which implies that the change in flow structure by the use of enhancer is much more significant as compared to property enhancement and slip mechanism by using nanofluids.
- Among all enhancers, the D-type wire coil shows a higher value of effectiveness than other configurations of the enhancers. As compared to the plain tube with DI water, the effectiveness of the double pipe heat exchanger enhances around 39.41 % using D-type wire coil and hybrid nanofluid.